LOW FREQUENCY VARIABILITY IN THE TROPICS AND EXTRATROPICS

Peter J. Webster

Department of Meteorology
The Pennsylvania State University
University Park, Pennsylvania, USA

1. INTRODUCTION

During the last decade, the ambitions of operational forecast centres have broadened with the extension of forecast range from days to weeks. With these new goals and increased expectations from the models, a whole new set of problems has emerged. Instead of just properly modelling the dynamics of the extratropics, which may have been sufficient for a forecast of a day or two duration, the phenomenology of the whole globe has now to be taken into account. With the extension of the forecast period, errors in one part of the globe appear to spoil forecasts of remote regions. Thus, for example, a proper parametrization of tropical convection becomes just as important to the prediction of weather over Europe as the observations over Europe itself. As the models are integrated for longer and longer times, forecasts also fall victim to the "climate drift" of the model where large errors tend to grow or congregate in specific regions due principally to model inadequacies. Also, it has become questionable whether an interactive lower boundary can be excluded from the operational models even for weekly forecasts.[1] Thus, as the forecast timescales increase, the same problems which plague climate modelling must be tackled and remedied by the operational modeller.

Figure 1 provides an indication of some of the problems associated with extended range prediction.[2] The analysis comes from the DERF data set which consists of 108 individual 30–day forecasts obtained using the U.S. NOAA National Meteorology centre (NMC) operational global model. The upper panels show the 108–day average of the initial analyses (i.e., the average of the day 0 fields of the 30–day forecast) of the 200 mb zonal and meridional wind component fields (U and V; Figs. 1a,b). The middle panels show the 108–day average of the forecast fields on day 30 of the forecast. while the bottom panels show the differences of the mean day zero and the mean day 30 fields. Collectively, these diagrams

[1] With certain phenomena, it may be that an interactive ocean boundary may be necessary for even shorter forecasts. An example may be hurricanes which severely perturb the upper ocean and modify the ocean-atmosphere fluxes.

[2] C. Reynolds; PSU/NMC, personal communication.

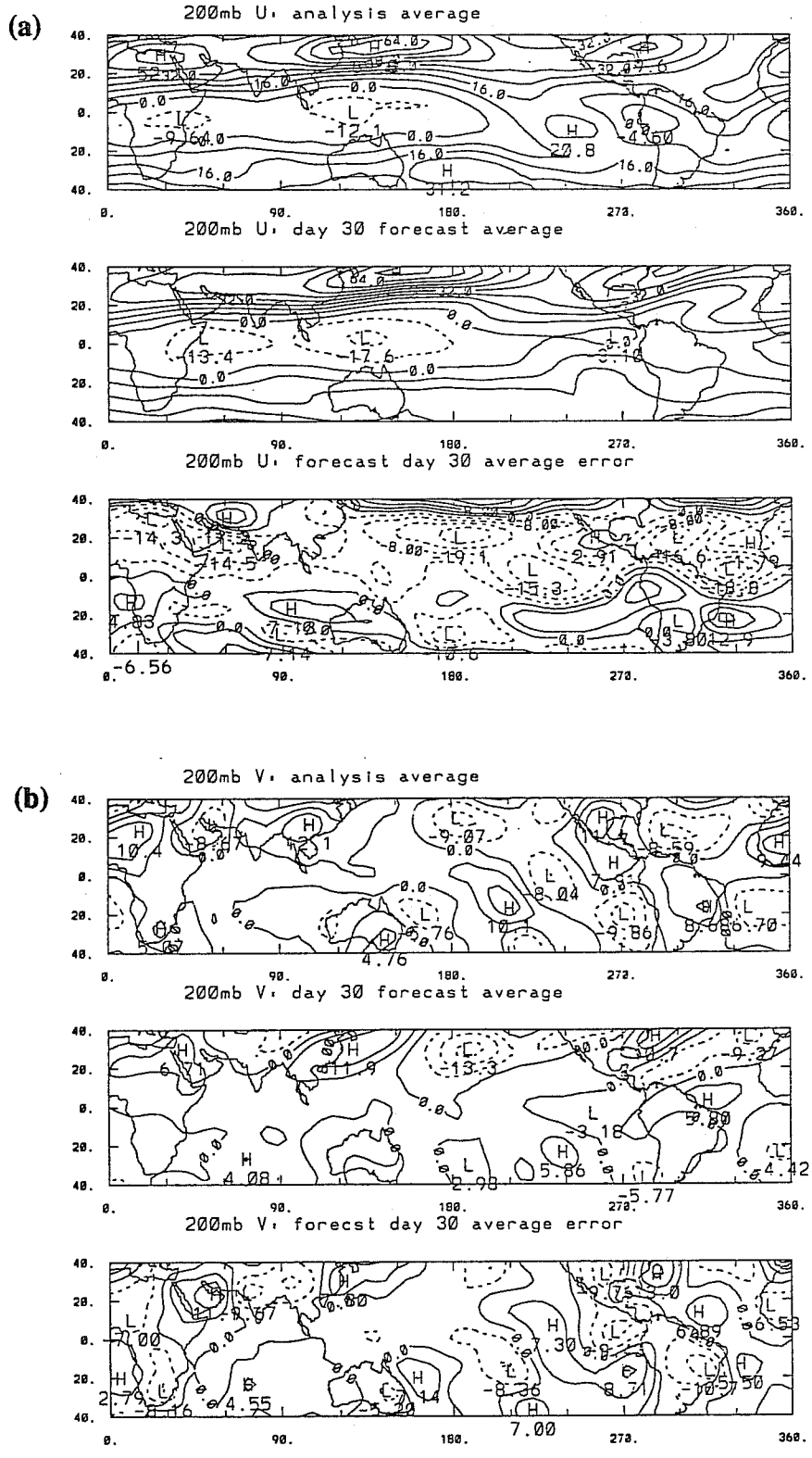

Figure 1: Climate drift of (a) the 200 mb zonal wind component and (b) the 200 mb meridional wind component in the NMC operational model as obtained from the DERF data set. The DERF data set consisted of 187 consecutive 30–daya forecasts. The upper panels show the 187–day average of the initial fields (i.e., day 0). The second panels show the average 30–day forecast. The bottom panels illustrate the mean climate drift or systematic error of the model which is given by the difference of the mean initial and the 30–day fields. (C. Reynolds, Pennsylvania State University. Personal communication)

provide an sense of the climate drift of the NMC model at that time. Some major aspects of the model climate drift are:

- Large difference fields exist in the tropical zonal wind component (Fig. 1a). The differences are negative suggesting that the model possess a strong easterly bias when averaged around a latitude circle.
- There are regions in the tropics where the climate drift is maximized. In particular, the zonal wind field is too easterly by over 15 ms^{-1} in the vicinity of the Pacific and Atlantic mid-ocean troughs. Fig. 1a (panel 2) shows that the upper-tropospheric westerlies in the Pacific and Atlantic oceans have nearly disappeared.
- Large errors are evident in the subtropical zonal wind fields (Fig. 1a) which arise from a polar displacement of the midlatitude jet streams.
- The 850 mb zonal winds show a small zonally averaged westerly bias (not shown). Considerable longitudinal structure exists especially in the regions below the mid-oceanic troughs indicating that the Walker Circulation has weakened considerably over the forecast period.
- The V difference fields (Fig. 1b) also show a very strong regionality in the tropics. Again, the largest differences occur in the vicinity of the mid-ocean troughs. In fact, in the Pacific Ocean an anomalous ridge is apparent indicating that the mid-Pacific trough has nearly disappeared.

Although these errors refer specifically to the NMC model used at the time of the DERF forecasts, they are very representative of the error fields found in most operational models.[3] For that reason, the error fields can be used as representative for discussion.

The importance of the systematic error depends, of course, on its magnitude relative to the variance of the quantity in question. Webster and Yang (1989) indicate that the variance of U in the equatorial 200 mb zonal wind component is of the order of 8 and 6.5 ms^{-1} in DJF and JJA, respectively.[4] Thus, the systematic errors are about a factor of two *larger* than the observed variance! Diagrams such as Fig. 1, therefore, present forecasters and other users of a model with a list of difficult questions.

- What is the cause of the model deviation? For example, are the locations of the extratropical jet streams a function of some scheme such as the local lower boundary model, problems with the way orography is handled in the model or because tropical heating

[3] The error fields refer to the NMC model used to create the DERF data set. Updated operational versions are now in use.

[4] Webster and Yang (1989) defined the variance as the power in transient motions on sub-monthly time scales.

is not adequately treated? Are the errors congregations closer to the equator the result of an inappropriate treatment of the interaction of the extratropics and tropics in the region of equatorial westerlies or some type of transmitted error from poorly represented convective or surface heating along the equator?

- Are the errors centres closer to the equator the result of an inappropriate treatment of the interaction of the extratropics and tropics in the region of equatorial westerlies or some type of transmitted error from poorly represented convective or surface heating along the equator?
- Why do errors appear to aggregate in particular regions, forming "error centres of action"?
- How meaningful are long term integrations or extended weather forecasts made with a model where the systematic error may be larger in certain regions than the local variance?
- How does one get rid a model of systematic errors?

Clearly, systematic errors are not just the problem of operational modellers. General circulation models used in climate simulations and experimentation (which are, in fact, much the same models but integrated for longer periods) also have errors associated with climate drift. A common strategy in climate modelling is to subtract a perturbed run (the experiment) from a control simulation in the hope that the climate drift is a systematic error and may cancel out. However, implicit in this assumption is that the systematic error behaves linearly and is a function of the model rather than the physical state simulated by the model. Thus, it is in the interests of modellers of many interests to identify the climate drift in a model, understand them and, thus, remove them.

A possible starting point in the analysis of the error fields may be the assessment of whether or not the error fields are a function of local inadequacies in the model or whether the errors are formed in some other region and propagate somewhere else where they may congregate or accumulate. That is, are the errors of Fig. 1 generated locally or are they forced at some remote location and are part of an "error teleconnection pattern". Such a determination would be useful as once an error source region is identified it may be possible to identify the offending process or parameter.

There are a number of ways which will help separate local and remote error sources. These are;

- The analysis of climate data: In Fig.1 we have noted that the patterns of systematic error tend to be localized. Diagnostic studies of real data have found that certain regions are more active than others and have used various techniques to establish causality. It is

important to examine the data to see if the model error patterns are similar to the climate anomaly patterns?

- Theoretical Studies: An examination of the theoretical basis for teleconnections of transient motions and of waves excited in different regions and of the processes which determine the mean (or slower evolving background state) may lead to an understanding of causality. The systematic errors grow rapidly. Is this growth the result *in situ* development or the propagating or advected effects of remote forcing or transient disturbances?
- Systematic experimentation with large scale models: Based upon hypotheses gained from diagnostic studies or theory, experiments can be made with a general circulation or an operational model, preferably in tandem with simpler prototypes or intermediate models.

We will now assess the low frequency variability of the tropics and extratropics using a combination of observational, theoretical and modelling studies. In the second section, we will look at evidence of low frequency variability in the tropics and extratropics. Next, we consider the phenomenology that occurs in the regions of error concentration along the equator noted earlier in Fig. 1. We then consider the role of heating in determing the location and intensity of the extratropical jets streams to test if misrepresentation of the heating is a candidate for the poorly located jet streams of the winter hemisphere. In the third section we will summarize the relationship between the slowly varying basic state and forced transients.

2. OBSERVED LOW FREQUENCY VARIABILITY

2.1 Long Term Variability of Low Latitude Flow

Figure 2 shows the distribution of the correlation coefficient between anomalies in the zonal component of the mean 200 mb velocity (U'; the derivation of U from its mean monthly value) at a reference point (150°W, 0°) relative to U' at all other grid points in the domain. The data set used is the NOAA/NMC mean monthly tropical strip winds.[5]

Figure 2a shows several major significant correlation areas in the tropics and middle latitudes. These are labeled as *A*, ... *E*. In the tropics the largest correlation centre is located in the neighborhood of the reference point *A*. A large negative region is located in the area between 330°E and 125°E (*B* and *C*). These correlation patterns along the equator infer that the variations of the zonal winds in the central-eastern Pacific are out of phase with the winds in the Atlantic and Indian Oceans, a phase difference that varies coherently in time along the equator. North and south of the reference point there are also two significant correlation

[5] As there is missing wind data in October and November, 1972, the U' data used to calculate the correlations are from December, 1972 through February, 1985, providing a sample of 147 monthly mean fields.

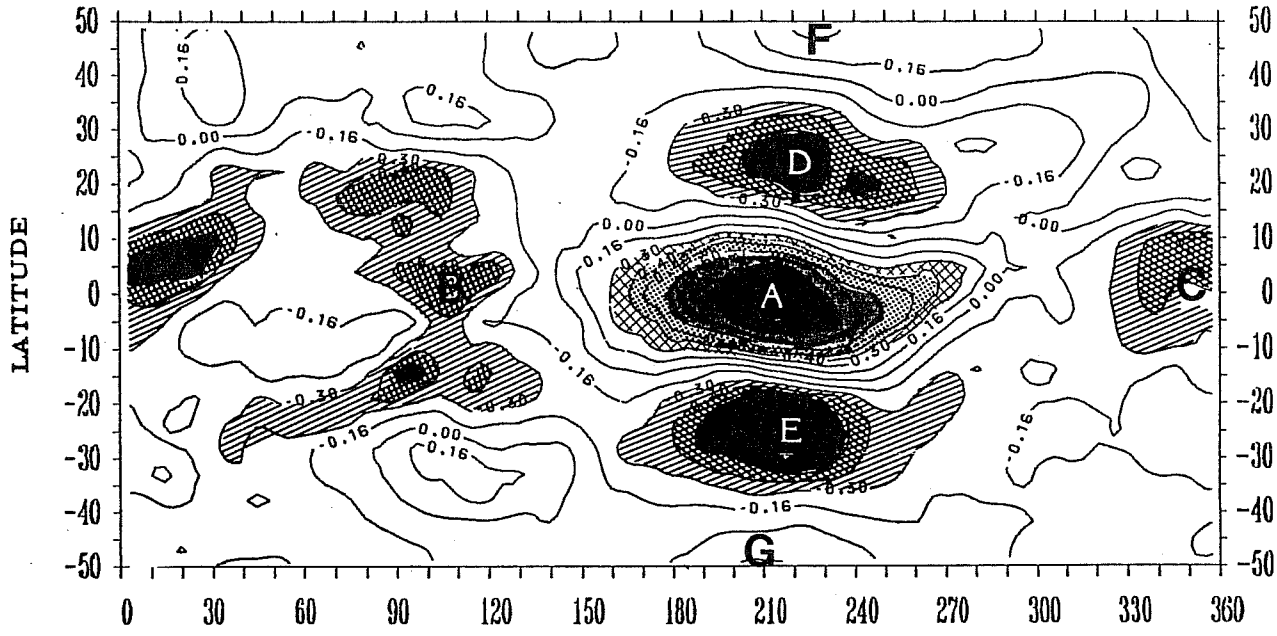

(b)

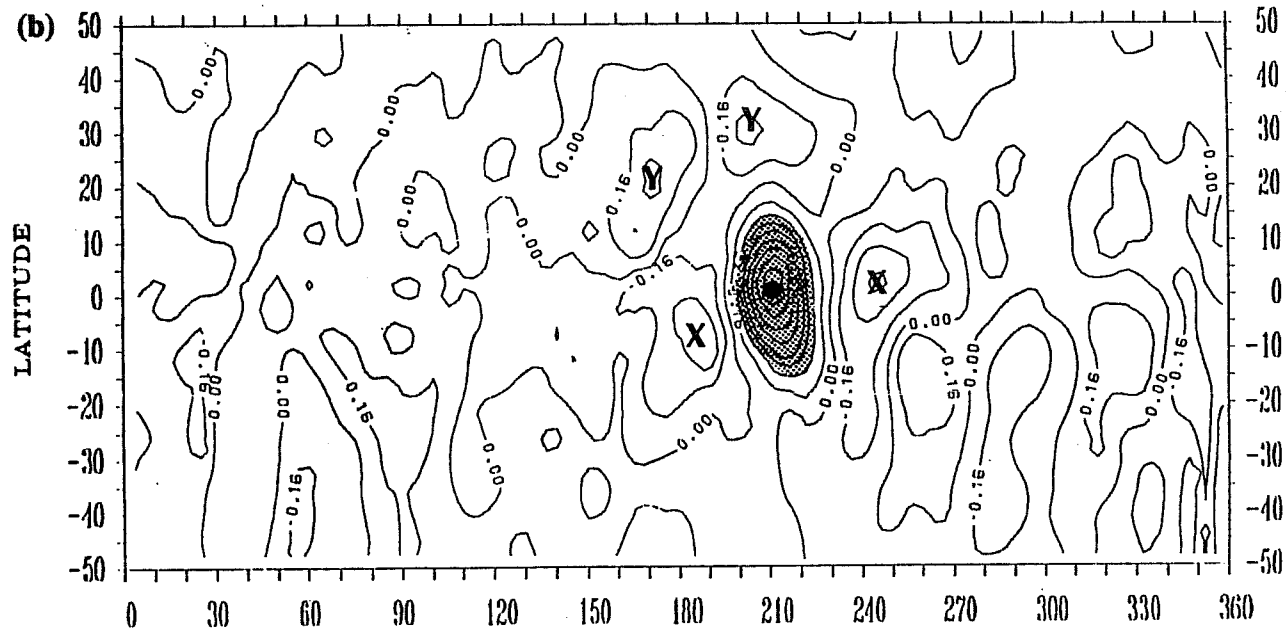

Figure 2: (a) The correlation fields of the *U* anomalies relative to the reference point (210°E, 0°N) marked *A*. The 95% confidence level is at ±.3. Areas greater than this level are shaded. Various correlation extrema are marked by letter and discussed in the text. (b) Same as (a) but for the *V* anomalies.

areas (negative) located to the north and south in the extratropical region around 220°E, 20-30°N/S (*D*) and indications of a further pair (*E*, positive) located even further poleward. This correlation pattern suggests that there exists wave propagation from the tropics to high latitudes (or reverse) with a lateral modal scale of roughly 40° to 50° of latitude.

Figure 2b shows an identical correlation map but for the 200 mb mean meridional wind component (V') with the reference point located at (210°E, 0°). The magnitude of the correlation fields turns out to be much smaller than those of U' and are less coherent. The region of coherence appears to be in the eastern Pacific Ocean spanning the equator labeled *X* for the negative centres and *Y* for the positive. The correlation pattern probably indicates changes in the location of the mid-Pacific trough. The largest negative correlation occurs between central-eastern Pacific and central-eastern Atlantic, i.e., between the regions 210°E-240°E and 0°-30°E.

The correlation centres D and E are tied to the low frequency Southern Oscillation Index (SOI).[6] Figure 3a shows the SOI for the period March, 1968 through February, 1985. Bjerknes (1966, 1969) related the Southern Oscillation Index of Walker to the variation of the sea surface temperature in the Pacific Ocean, defining, thus, the Southern Oscillation-El Niño (ENSO) phenomena. Periods of negative SOI (e.g., 1968-1969, 1972-1973, 1977-1978, 1982-1983) correspond to warm events or El Niño periods in the tropical Pacific Ocean. Strongly positive SOI years are periods of La Niña (e.g., 1971, 1974, 1976)

Figure 3b shows time-longitude plots of $\bar{U}$ averaged between 25°N and 35°N, 5°N and 5°S and 25°S, and 35°S for DJF from 1965 through 1985. In the equatorial belt, the magnitude of the winds oscillate considerably with maxima and minima associated with positive and negative values of the SOI. At higher latitudes in both hemispheres, near-simultaneous variations in the zonal wind field occur. Figure 3c shows the corresponding boreal summer sections. Large interannual excursions appear in the wintertime southern hemisphere with an apparent relationship to the SOI. With the SOI $<< 0$, the jet intensifies and extends eastward. Although the winds are much lighter in the summer hemisphere, the jet maxima, although fairly weak, is further poleward than the 25°–35°N section. However, considerable variability, again apparently associated with the SOI, may be seen in the vicinity of the mid-Pacific trough.

To study the latitudinal correlation structure in more detail, the reference correlation point is moved along the equator and examine the individual meridional correlation strip maps at each latitude is examined. Meridional strips are defined between 50°N and 50°S and are averaged over 60° of longitude about a particular reference point. Fig. 4a shows the

[6] The SOI is usually defined as the normalized pressure difference between Tahiti and Darwin and provides a measure of the macroscale variability of the tropics.

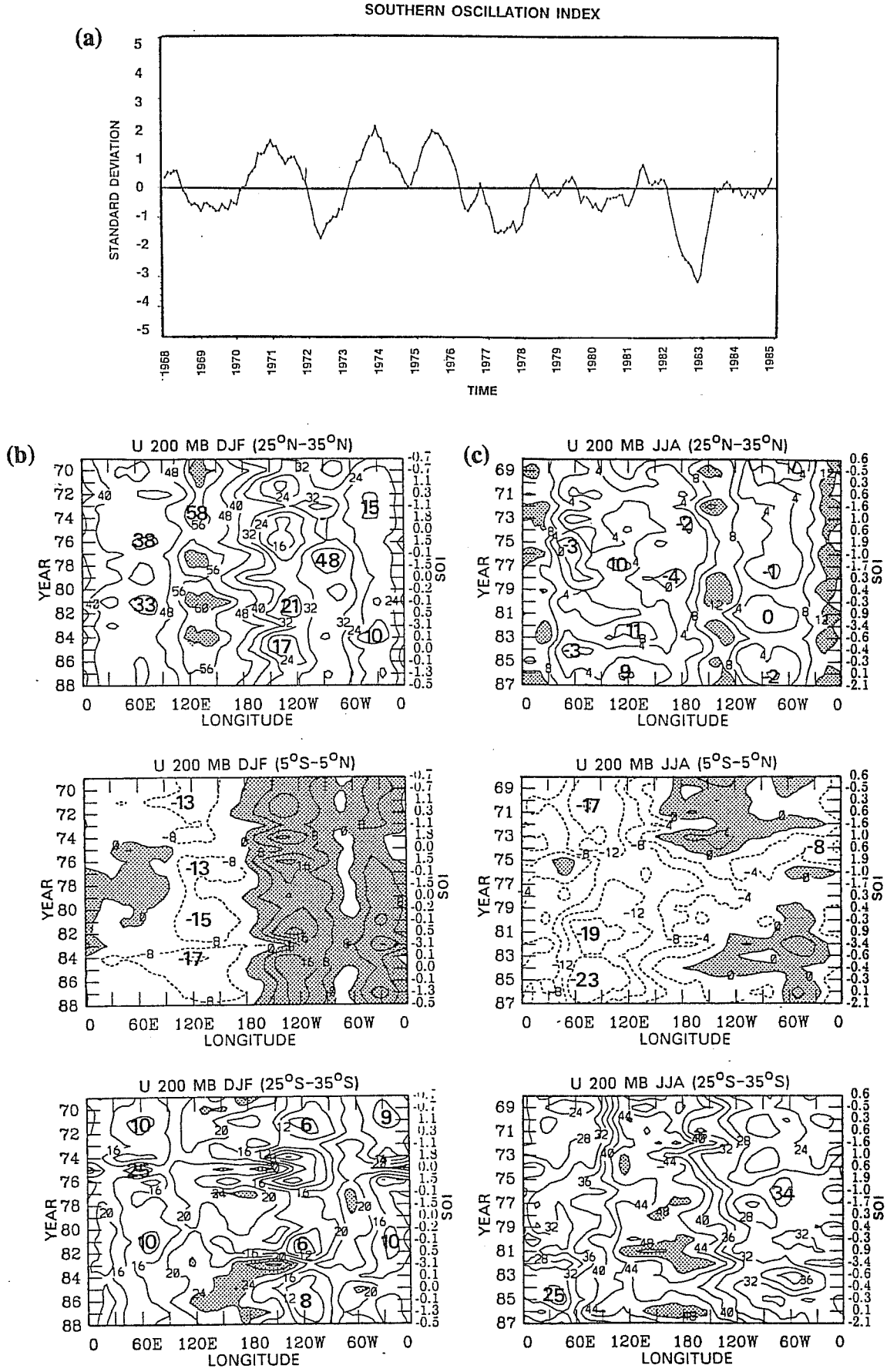

Figure 3: (a) The Southern Oscillation Index (SOI) for the period 1968 t0 1985. The SOI is approximately the normalized pressure difference between Tahiti and Darwin. (b) Time-longitude section of the zonal wind in three latitude bands 25°N–35°N, 5°N-5°S and 25°S-35°S for DJF. The mean seasonal SOI is listed on the left ordinate. (c) Same as (b) except for JJA. Strong westerlies or easterlies are shaded.

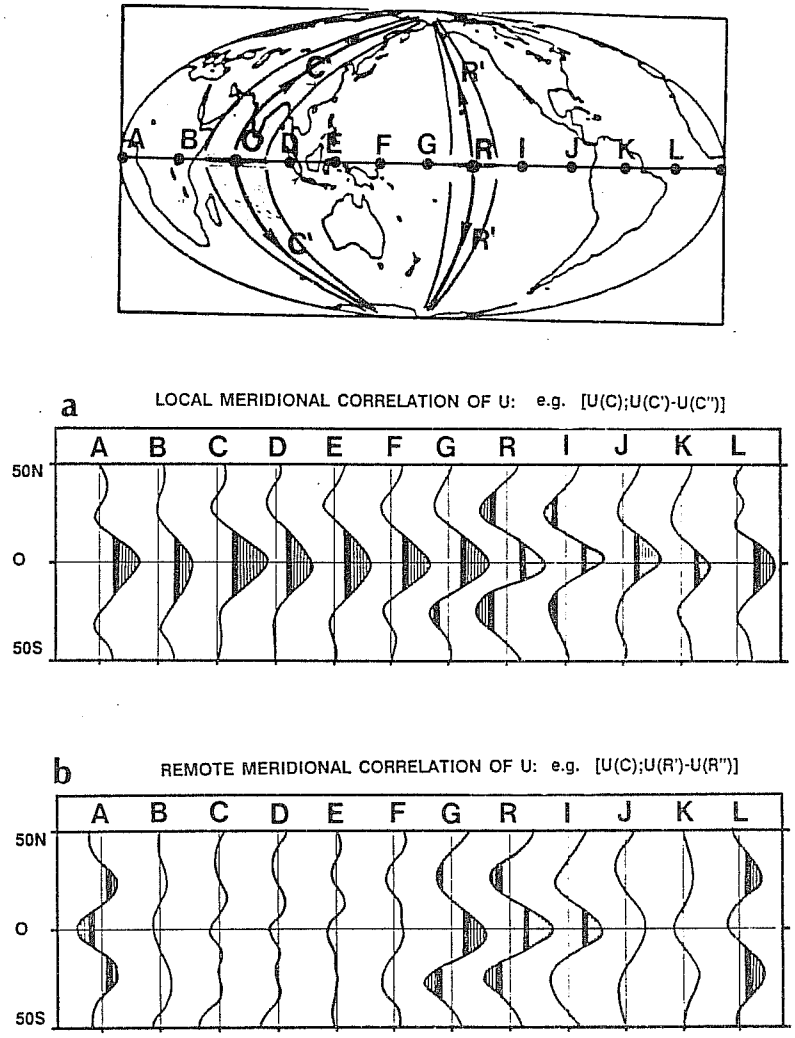

Figure 4: (a) "Local" correlation curves indicating the correlation of U averaged in 30° longitude strips as a function of latitude. Reference points are located on the equator at 0, 30°E, 60°E and etc.. The correlation scheme is summarized in the upper diagram. Shaded parts of the curve denote statistical significance >95%. (b) Same as (a) except for "remote" correlation curves indicating the correlation of U averaged in 30° longitude strips about the 210°E longitude strip relative to the variation of U at points 0°, 30°E, 60°E and etc., along the equator.

distribution of correlations between U anomalies about a series of reference points and the U anomalies in the longitudinal strip at all other grid points to the north and south. The upper panel describes the scheme. The curves represent the local correlations of the U anomalies at (say) point C with those along the *local* meridian C'-C'. The shaded regions denote statistical significance beyond 95%. Similar patterns appear at all longitudes (i.e., negative correlation between the tropics and high latitudes) although *only in the vicinity of the upper tropospheric westerlies* (i.e., 150°E to 120°W) *are the correlations strong and significant away from the equator*!

Figure 4b shows the results of an examination of the "remote" tropical-midlatitude correlation. Here we plot the correlation of U at a reference point in a particular longitude belt along the equator with the U variation along a longitude-latitude strip to the north and south of the mid-Pacific westerly maximum, specifically in the band between 180°E and 240°E. I.e., relative to the schematic diagram at the top of the figure, the strips show the variation of the correlation of (say) point C with the 30° averaged correlations along R'-R'. *Strong associations exist in strips between 330°E and 30°E and the extratropics in the reference zone to the north and south of 240°E even though the reference point and reference zone are removed by 180° of longitude!* That is, the correlation between the U-variation along the equator at 0°E is much more strongly coupled with the middle latitudes 180° of longitude *removed* away from the correlation point than is related to variability immediately to the north and south.

2.2 Mean Flow, Transient Energy Relationships

Webster and Yang (1989) compared the vertical structures of the mean perturbation kinetic energy (*PKE*)[7] and zonal wind fields. The quantities were averaged between 25°N and 35°N and 5°N and 5°S for DJF and are shown in Figs. 5 and 6, respectively. In the extratropics, the *PKE* maxima are located between 300 and 200 mb, the height at which the maximum westerlies are found. Great similarity exists between the shapes of the *PKE* and U except that the maximum *PKE* centres are just downstream of the westerly maxima. The structure of the U and *PKE* fields can be examined further by removing the zonally averaged values at each height. These "starred" quantities show a minimal tilt with height of both quantities.

In Fig. 6, the mean OLR along the equator is plotted together with the U and *PKE* fields. The U-fields show an out-of-phase structure between the lower and upper troposphere in sharp contrast to the in-phase structure found in the extratropics. Equatorial westerlies extend between 500 and 100 mb in the western hemisphere but are confined to below 700 mb over the Indian Ocean and the western Pacific Ocean. Two westerly maxima exist over

[7] *PKE* is defined as $PKE = \overline{(u'^2 + v'^2)}/2$.
The primed quantities refer to temporal deviations from the monthly mean NMC data. Thus *PKE* is a measure of the kinetic energy of phenomena with sub-monthly timesacles.

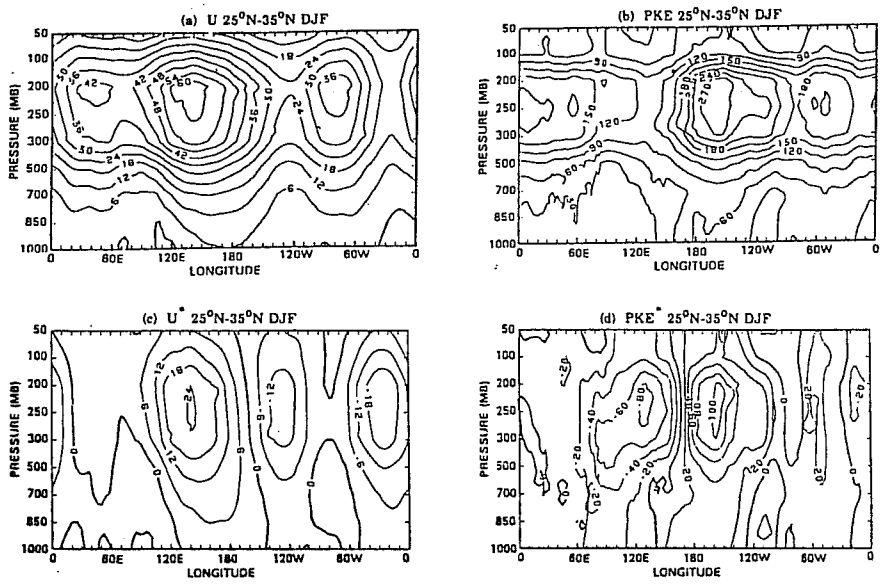

Figure 5: Vertical section of quantities averaged in the latitude band 25°N-35°N for DJF. (a) and (b) show the *U*-field and the *PKE* and (c) and (d) show the same fields but with the zonal average removed (U^* and PKE^*). From Webster and Song (1989).

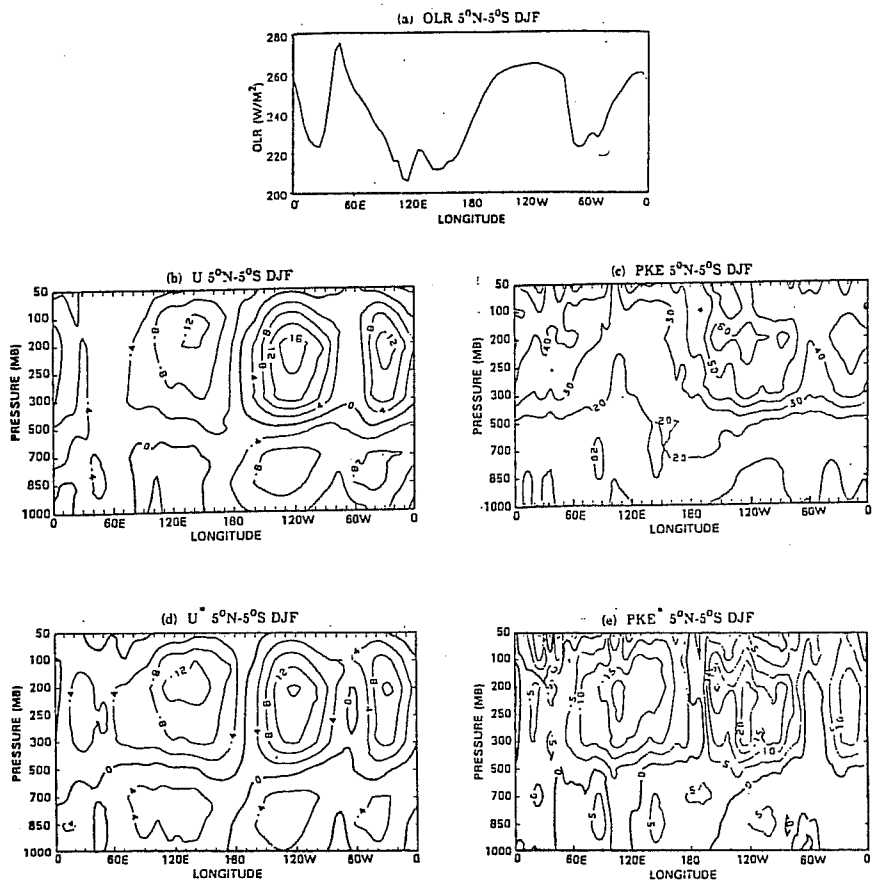

Figure 6: Same as Fig. 5 except for the latitude band 5N-5S. The mean OLR in the band is shown in the upper panel with an inverse scale. From Webster and Yang (1989).

the eastern Pacific Ocean and the Atlantic. Easterly winds exist elsewhere and, together with the westerlies, clearly defining the "Walker Circulation" along the equator. The removal of the zonal average (lower panels) discloses two cells, the stronger being consistent with the ascent over the warm pool regions of the western Pacific Ocean and with the OLR minimum (top panel). In the upper troposphere, the *PKE** maximum occurs in the vicinity of the westerly maxima or in the location of OLR maxima. The *PKE**minimum, on the other hand, is colocated with the maximum easterly. In the lower troposphere, the same associations are found. Thus, we have the strange result where maximum transient activity (at least in the mean) occurs where the convection is a minimum. On the other hand, where there is maximum convective activity there is a minimum in the transient activity.

In the extratropics, the location of the *PKE* maxima (which is downstream of the *U* maxima) suggests that the *PKE* are produced by hydrodynamically unstable processes which would be consistent with the smaller vertical tilt of the perturbation compared to the tropics. In the tropics, the locations of the *PKE* may be assumed to be a measure of the activity of the propagating disturbances from the extratropics to the tropics through the westerly duct in the manner of Webster and Holton (1982) or the accumulation of energy as suggested by Webster and Chang (1988). Alternatively, it could be the combination of both effects which need not be mutually exclusive.[8] To test for consistency with the accumulation theory, *PKE** and U_x^* distributions were compared. These are displayed in Fig. 7 and show a fairly strong relationship. In winter, the *PKE* maxima over the centre-eastern Pacific Ocean and the Atlantic ocean are colocated with the maximum negative longitudinal stretching deformation. In summer, the deformation field is much weaker and, although the *PKE* is weaker as well, there is still a weak correlation between U_x^*.

2.3 Relationships Between Tropical Heating and Extratropical Jets

The question arises as to whether it is feasible that specific phenomena in one hemisphere can be influenced by specific forcing in the other hemisphere but away from the westerly duct? There are clear examples of variations of heating occurring on a multitude of time scales but what effect do they have on remote events in the other hemisphere? In particular, do relationships exist between the location and the intensity of the winter hemisphere jet streams and the heating in the other hemisphere? This question requires some consideration as a number of studies (e.g., Blackmon et al., 1977) have shown that the jet streams are source

[8] Webster and Chang (1988) eliminated the possibility that local hydrodynamic instabilities in the equatorial westerlies produce the PKE maximum by conducting a series of experiments with random forcing in a relatively realistic $U(x,y)$ flow. In the equatorial region all of the perturbations damped out.

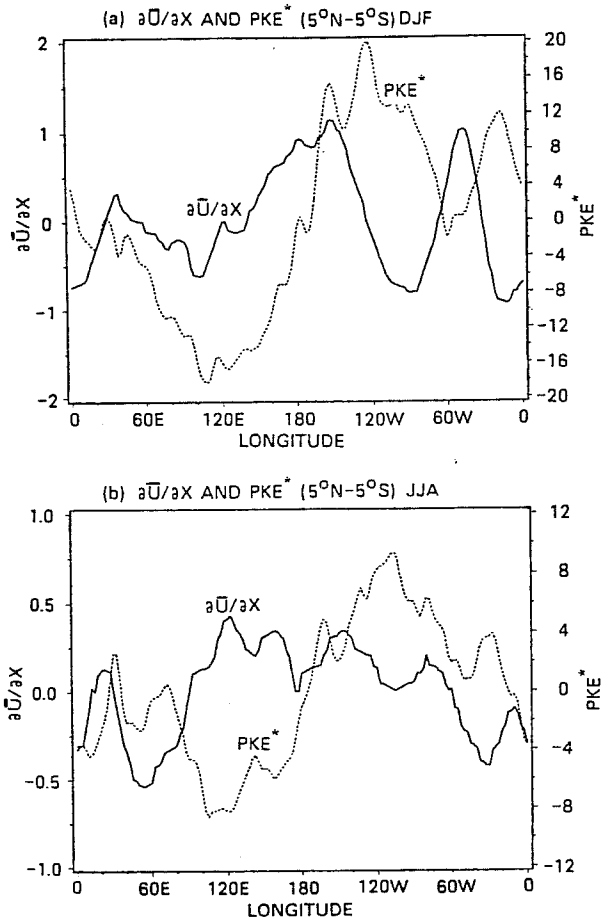

Figure 7: Plot of the longitudinal stretching deformation U_x and *PKE** in the 5N-5S band for (a) DJF and (b) JJA. Note change of scale between the two figures. From Webster and Yang (1989).

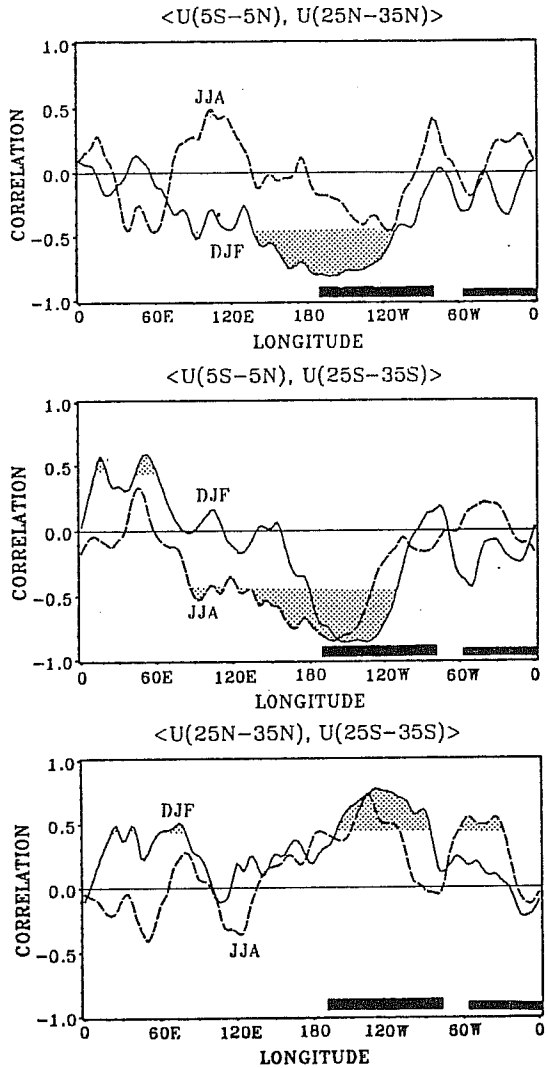

Figure 8: Simultaneous correlations between U in two different latitude bands for DJF and JJA. Values with >95% significance are shaded. Thick bars signify extent of westerlies along equator during DJF. Easterlies prevail during JJA.

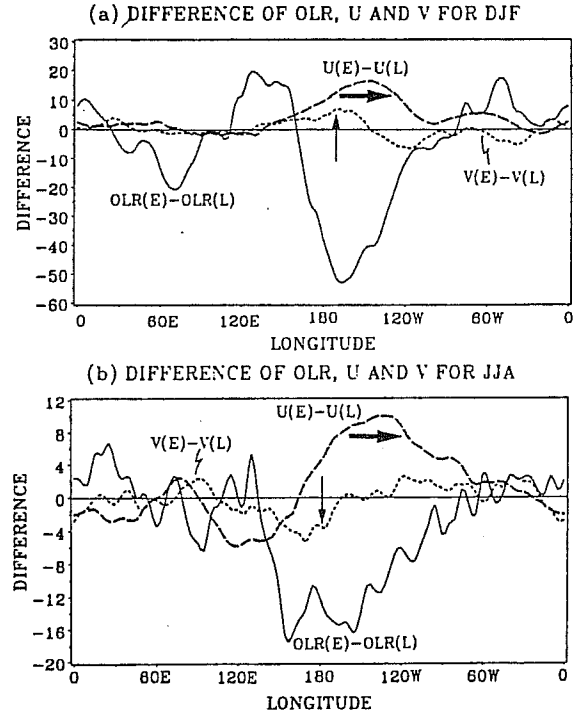

Figure 9: Difference fields (El Niño minus La Niña) of OLR, 200 mb V and U for (a) DJF where OLR, V and U are averaged between 0°–10°S, 15°N-25°N and 30°N-40°N, and (b) JJA where OLR, V and U are averaged between 0°–10°N, 15°S-25°S and 25°S and 35°S. The thick arrows indicate the eastward migration and downstream strengthening of the jets; the thin arrows show the eastward migration and weakening of the subtropical meridional winds. From Yang and Webster (1990).

regions of extratropical storms. Thus, variations in the jet stream position and intensity may have a significant impact on the weather of the winter hemisphere.[9]

Figure 8 shows the simultaneous correlations of the $\bar{U}$ field between 5°N-5°S and 25°N-35°N (top panel), between 5°N-5°S and 25°S-35°S (middle panel), 25°N-25°N and 25°S-35°S (lowest panel). The longitude belts corresponding to the DJF tropical westerlies are marked with heavy lines. Correlations passing the 95% significance level are shaded. In both DJF and JJA, the strongest correlations occur over the central-eastern Pacific Ocean, where tropical westerlies prevail in DJF and relatively weak tropical easterlies appear in JJA. The correlations between the tropics and extratropics are stronger in DJF than in JJA in the northern hemisphere, although they are similar in magnitude in both seasons in the southern hemisphere. A strong negative correlation is shown clearly over the central Pacific Ocean in the upper and middle panels; stronger (weaker) equatorial westerlies and weaker (stronger) equatorial easterlies are accompanied by weaker (stronger) extratropical westerlies in both hemispheres. Thus, an in-phase change occurs in the extratropical westerlies over the central Pacific Ocean of both hemispheres. Note, too, the strong positive correlations in the lower panel. Although somewhat weaker, negative tropics-extratropics correlations are found over Asia in DJF and over the southern Indian Ocean in JJA, which show the relationship of the extratropical westerly jet streams to the tropical easterlies. In turn, the tropical easterlies are closely associated with the diabatic heating maximum over the eastern Indian Ocean and the western Pacific Ocean. In summary, the maximum cross-equatorial correlation occurs in the region of Webster and Holton's (1982) "westerly duct". Also, substantial correlations, although relatively weaker, occur between the strength of the equatorial easterlies and the extratropical westerlies along the equator.

Because of the seasonal differences in the jetstream locations and their interannual variability, the variations which appear in Figs. 3 and 8 are difficult to ascribe just to orography except through a very a convoluted chain of events. Yang and Webster (1990) shows strong coherence between variations of the heating in the summer hemisphere with changes in the flow in the winter hemisphere. Such features are summarized by the composites show in Fig. 9a and b for winter and summer. During the El Niño years, the Australian jet stream

[9] Whether orographic or thermal forcing is the dominant process in determining the location and magnitude of extratropical stationary waves has been the subject of much discussion and debate. For example, Charney and Eliassen (1949), Bolin (1950), Manabe and Terpstra (1974), Held (1983), Wallace (1983), Jacqmin and Lindzen (1985), and many others, claimed that the effect of topography is primary and instrumental in forcing stationary waves. Clearly, there is theoretical evidence to support such an important role for orography. For example, the study of Held (1983) using a hemispheric barotropic model with only orographic forcing found zonal wind maxima downstream of the major northern hemisphere orographic features. Chen and Trenberth (1988) with a steady state hemispheric model, produced solutions that matched the mean structure of the northern hemisphere by including a feedback for perturbations produced by the heating differentials to interact with the orography. Both the Held and the Chen and Trenberth studies precluded the possibility of cross-equatorial flow and interhemispheric interaction through the geographic limitations of their models.

moves significantly when the subtropical meridional winds (the poleward winds over the southern Indian Ocean and the eastern Pacific Ocean, and the equatorward winds over the central Pacific Ocean) shift eastward and decrease in magnitude. These changes appear to be associated with the eastward migration of the heating in the other hemisphere. It is worthy reemphasizing that the upstream weakening of the Australian jet in the El Niño years is more distinct than the Asian jet in DJF and that the changes in the meridional winds over the Pacific Ocean reflect the changes in the mid-Pacific trough.

2.4 Summary

The observational studies discussed in the preceding paragraphs indicate the there is considerable coherent variability between the tropics and the extratropics and between the subtropics of the two hemispheres. One particular point emerges continually. The central Pacific Ocean, in particular, and the Atlantic Ocean to a lesser extent (except during El Niño periods where the activity in the two regions is reversed), appear as loci for propagating tropical and extratropical disturbances. As these regions appear to be active across a wide frequency range it would appear that successful modelling of the global weather or climate that they be carefully modelled. Unfortunately, Fig. 1 indicates that these same regions are where the models tend to do worst.

3. STRUCTURE OF LOW FREQUENCY PHENOMENA

Since the 1960's, through a combination of theoretical and modelling studies, there has been a substantial increase in the understanding of the structure of the tropical atmosphere, its elementary physical nature and the interaction between the tropics and extratropical regions. Using a simple primitive equation free-surface barotropic model on an equatorial β-plane, Matsuno (1966) described theoretically the fundamental normal modes of the tropical atmosphere including equatorially trapped eastward propagating Kelvin waves and mixed Rossby-gravity waves and westward propagating Rossby waves. These modes were soon identified in the stratosphere and troposphere by Yanai and Maruyama (1966), and many others, using diagnostic methods. The identification of equatorially trapped modes was important as the impact of the tropical atmosphere on the general circulation and the interaction between the tropics and mid-latitudes had been hinted at by many meteorologists but never formally formulated. A number of recent theoretical works and general circulation model studies (e.g. Simmons *et al.*, 1983; Webster and Chang, 1988; Chang and Webster, 1990; Zhang and Webster, 1989 and others) have provided frameworks for evaluating effects of tropical forcing on the extratropical circulation. For example, Simmons *et al.*, (1983) see

the evolution of teleconnections patterns resulting from slow instabilities of the dimensional, global scale basic flow. The Webster-Chang-Zhang studies, on the other hand, emphasize the importance of the structure of the slowly varying background state on the characteristics of transient waves.

Despite many theoretical and observational advances, there are still some aspects of the structure of low-frequency waves in the tropics and the interrelationship of the tropics and the extratropics that are not fully understood. For example;

- Can a Rossby wave-train emanate from all regions of the tropics or only from a particular region as suggested theoretically for the subseasonal time scales by Webster and Chang (1988)?
- Where do the concepts of Sardeshmukh and Hoskins (1988) who feel that nonlinear aspects of the divergent flow provide a local source of waves to middle latitudes from the easterlies themselves?
- How do the El Niño or warm events affect the structure of the low-frequency tropical transients in their form and in the manner in which they interaction between the tropics and the extratropics?
- How important is the mixed Rossby-gravity wave in the transient dynamics of the tropical atmosphere?
- Are there low frequency modes or mechanisms of communication with the period longer than 40-60 days? If they exist, what role do they play in the general circulation and in the change of climate?
- Do the "fast teleconnections" of Chang and Webster (1990), (i.e., periods < 40-60 days) rectify to provide a coherent response in the mean?

3.1 Characteristics of the Basic Flow at Low Latitudes

Fig. 10 which plots the mean boreal winter 200 mb flow. While it is possible to segregate the tropics into the broad categories of easterlies and westerlies, it should be noted that tropical easterlies tend to be associated with extremely strong latitudinal shear and tropical westerlies with weak shear. The association leads to two further circulation categories, *EE* and *EW*, shown in the bottom panel of Fig. 10. The middle panel shows a cross-section of the mean flow along the equator. The most notable feature is that the upper and lower tropospheric flow is almost exactly out-of-phase. Clearly, the behavior of tropical modes in these complicated flows will require careful examination.

In the following paragraphs we will describe some of the essential elements which determine the structure of equatorial modes in a highly variable basic state. In particular;

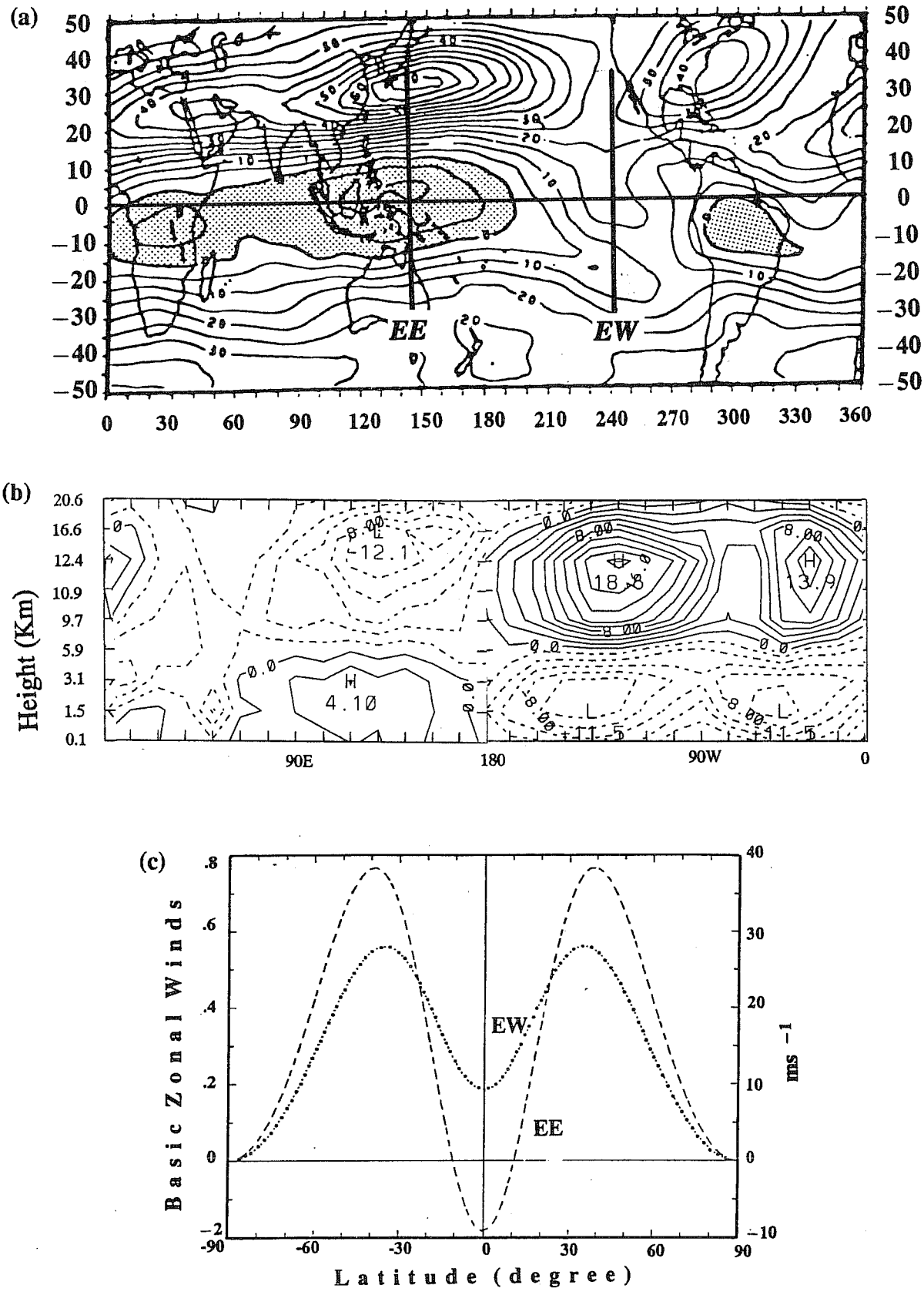

Figure 10: (a) The long term average DJF *U*-field at 200 mb. Regions of easterlies are shaded, (b) Vertical cross section of U along the equator, and (c) Idealized sections of *U* along the meridians marked in (a). The two sections pass through very high shear regions (EE) and weak shear (EW) associated with the equatorial westerlies.

- Constant basic flows; U=constant,
- Zonally symmetric shear flows; $U=U(y)$,
- Flows with longitudinal stretching deformation: $U=U(x)$,
- Flows with longitudinal stretching deformation and vertical shear: $U=U(x,z)$,
- General two-dimensional flows; $U=U(x,y)$.

3.2 The Basic System

We define a linear, inviscid flow on an equatorial β–plane with a general basic flow $U=U(y)$. To consider flows like $U(x,z)$ we will need to make the model more general. The total geopotential field of the system can be expressed as:

$$\begin{aligned} \phi(x,y,t) &= \Phi_0 + \Phi_s(y) + \phi(x,y,t), \\ \Phi_0 &= \text{ constant}, \\ \frac{d\Phi_s}{dy} &= -fU \\ \Phi_0 &>> \Phi_s. \end{aligned} \tag{1}$$

We can write the shallow water equations in nondimensional form as:

$$\begin{aligned} u_t + \underline{Uu_x} + [vU_y] - \overline{yv} + \phi_x &= 0 \\ \overline{v_t} + \underline{Uv_x} + yu + \phi_y &= 0 \\ \phi_t + \underline{U\phi_x} - [yUv] + (u_x + v_y) &= 0. \end{aligned} \tag{2}$$

A nonzero basic state produces Doppler terms (underlined) and non-Doppler terms (brackets). The usual long wave approximation (overline) is not made, as in a flow with $U(x)$ there is the possibility of long waves reducing their horizontal scales substantially, thus rendering the approximation invalid. However, we will discuss this approximation later.

Assuming normal mode solutions proportional to $\exp i(kx - \omega t)$ and making a number of transformations, we can write a governing wave equation in the meridional velocity component as;

$$V_{yy} + \Gamma^2(y)V = 0 \tag{3}$$

where $\Gamma^2(y)$ is the refractive index squared.

At the latitude where $\Gamma^2(y)$=0, (i.e, at $y=y_t$) the form of the solution changes from wave-like to evanescent. y_t is thus the wave turning latitude. Equatorial trapping requires, thus, that Γ^2 change sign somewhere between the equator and the pole. The refractive index

squared is given by

$$\Gamma^2 = \tilde{\omega}^2 - k^2 - \frac{k}{\tilde{\omega}} - \left\{1 + \frac{k}{\tilde{\omega}^2}U + \frac{U^2}{4}\right\}y^2 - \frac{1}{2}U - \frac{3k^4}{\tilde{\omega}^2 - k^2}(U_y)^2$$
$$- \frac{k^3}{\tilde{\omega}(\tilde{\omega}^2 - k^2)}U_{yy} + \left\{\frac{1}{2} - \frac{k^3}{\tilde{\omega}(\tilde{\omega}^2 - k^2)} - \frac{2k^2}{\tilde{\omega}^2 - k^2}\right\}yU_y \qquad (4)$$

where

$$\tilde{\omega} = \omega - kU \qquad (5)$$

is the Doppler shifted frequency. The non-Doppler terms in Γ^2 are underlined. In general form we may write

$$\Gamma^2(y) = (a - by - cy^2) \qquad (6)$$

where a contains the Doppler terms and b and c the non-Doppler terms.

3.3 Doppler and Non-Doppler Effects

Figure 11 shows the dispersion curves for equatorial modes for the simple case when U=0. The heavy solid curves correspond to Matsuno's solutions but for a fluid with an equivalent depth of 300m. It is not entirely obvious what changes would result to the dispersion curves if a non-zero basic state were introduced as both Doppler and non-Doppler terms have been identified in *(2)*. If the Doppler terms dominate, the impact of a nonzero basic state will be merely to shift the curves up or down (i.e., a "DC" shift) shown as the dotted line in Fig. 11 for the n=1 Rossby mode. However, if the non-Doppler effects become important then the modification will be more complicated. For example, the non-Doppler modification of the n=1 mode may look like the dashed-dotted curve.[10]

3.4 Modal Structure in Complicated Basic States

(i) Constant Basic Flows: U=U_0

Following Zhang and Webster (1989), it can be shown that for a constant zonal mean flow that the coefficients of *(6)* become:

$$a = \tilde{\omega}^2 - k^2 - \frac{k}{\tilde{\omega}} - \frac{U}{2}$$
$$b = 0 \qquad (7)$$
$$c = \left(1 + \frac{kU}{\tilde{\omega}} + \frac{U^2}{4}\right)y^2$$

[10] A brief discussion is given regarding the inappropriateness of the 'long-wave approximation" is given in Appendix 1.

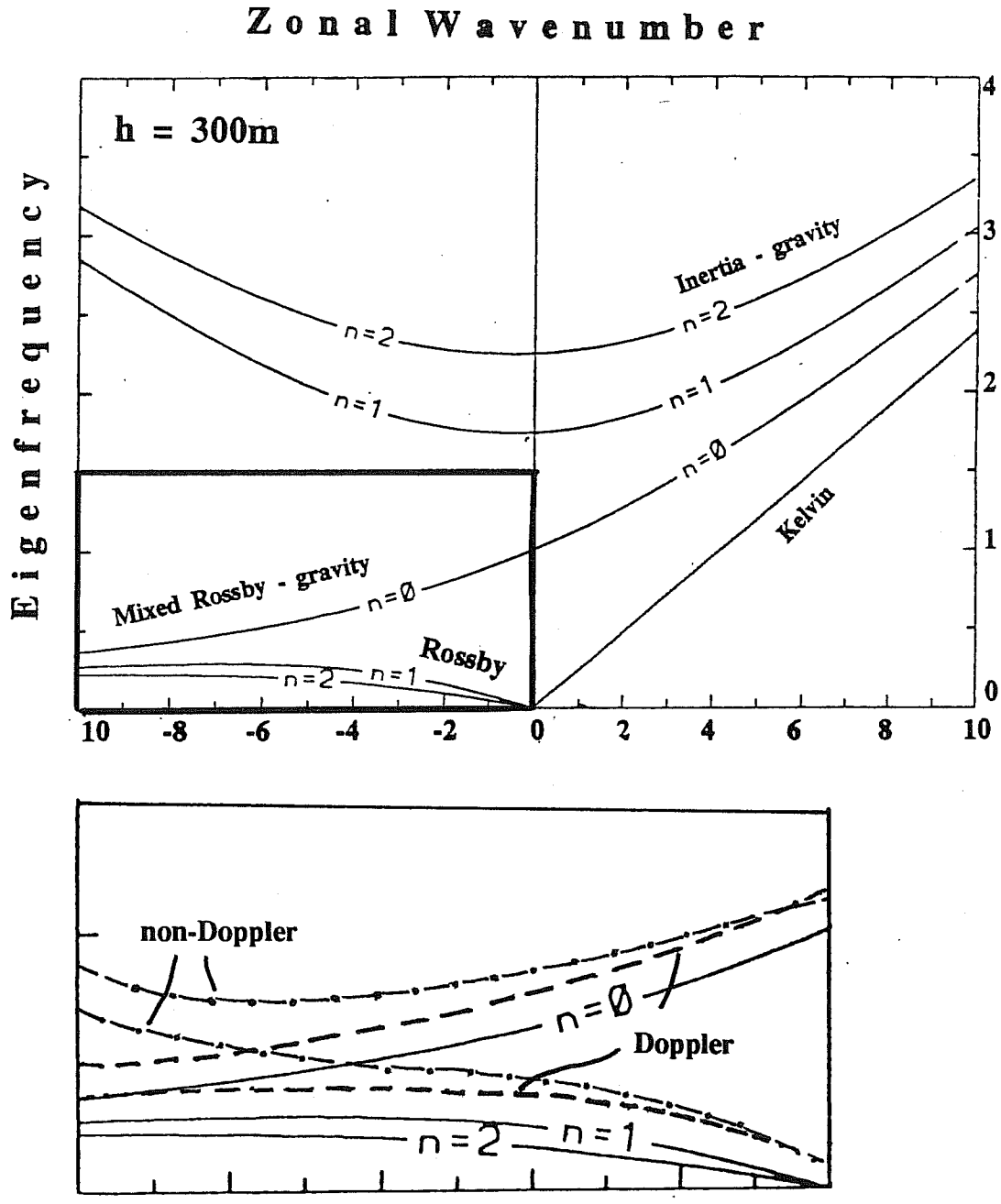

Figure 11: Dispersion curves for the equatorial waves. Labels denote the families. Inset area on lower left shows the possible effects of Doppler and non-Doppler shifting of the modes. A pure Doppler shift will move all the eigenfrequency curves an equal amount which is proportional to the basic wind speed independently of wavenumber or mode (dashed curves). A non-Doppler shift will move the curves as either a function of wavenumber or nonlinearly as a function of wind strength (dash-dotted curve).

and the refractive index squared reduces to:

$$\Gamma^2(y) = \tilde{\omega} - k^2 - \frac{k}{\tilde{\omega}} - \left(1 + \frac{kU}{\tilde{\omega}}\right)y^2 + ... \qquad (8)$$

so that general solutions possess the form;

$$\begin{aligned} v(y) &= H_n\left(K^{1/4}y\right)\exp\left(-\frac{K^{1/2}}{2}y^2\right), \\ \tilde{\omega}^2 - k^2 - \frac{k}{\tilde{\omega}} &= (2n+1)K^{1/2}, \\ y_t &= \pm(2n+1)^{1/2}R, \\ K &= \left(1 + \underline{\frac{kU}{\tilde{\omega}}}\right). \end{aligned} \qquad (9)$$

where R is the Rossby radius of deformation. The non-Doppler terms, identified in basic set *(2)* are manifested in the solution as the underlined term in the K definition. Thus, we would expect the non-Doppler to alter the structure of the solutions and the eigenfrequencies as a function of the horizontal scales n and s. Examination of K suggests that the changes to the solutions will not be symmetric for positive and negative values of U.

Figure 12 summarizes the impact of a constant zonal current on the equatorial modes. The effect of the non-Doppler terms on the distribution of the eigenfrequencies of the n=1 Rossby mode is shown in Fig. 12a for three values of the constant zonal flow: U= 10, 0 and –10 ms^{-1}. Clearly, as k increases, the impact of the non-Doppler terms increases substantially. For a given scale, the frequencies tend to be larger than the U=*0* for U>0 while the opposite appears true for the U<0 case. To illustrate the effect of the basic state on the latitudinal scale of the equatorial mode, the Rossby radius of deformation is plotted in Fig. 12b for the n=1 mode. When U>0, R increases while when U<0, R decreases. In other words, westerlies tend to decrease the trapping of equatorial waves while easterlies tend to enhance the trapping.[11] The change in trapping is emphasized as k increases, especially in a westerly basic state. Figure 13 shows the structure of the zonal wind of the Rossby modes n=*1, 2*, k=*5* for the different values of the basic state. The mode is much more tightly confined to the equatorial regions in the easterlies than in the westerlies.

(ii) Zonally Symmetric Shear Flows: U=$U(y)$

In order to assess the importance of shear, and to see if the effects of a constant basic flow noted in (a), above, would be modified by shear, Zhang and Webster (1989) studied the structure of equatorial modes in a flow U=$U(y)$. Two configurations of shear flow were considered; the *EE* and *EW* of Fig. 10.

[11] The physical basis of why the background basic state determines the degree of trapping is shown in Appendix 1.

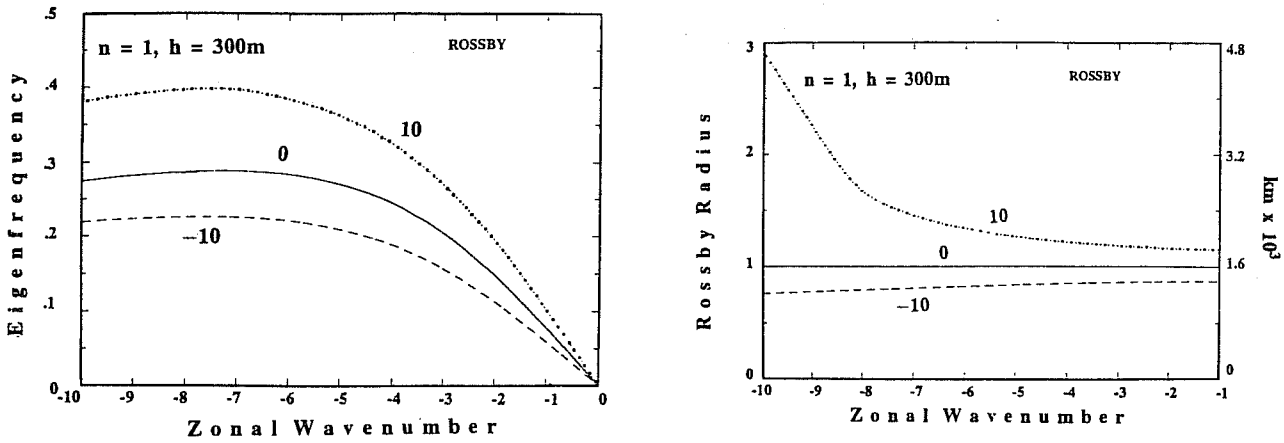

Figure 12: Examples of the non-Doppler effects introduced into the system by constant basic flows of –10, 0 and 10 ms^{-1}. Left hand panel shows the variation of the n=1 Rossby mode eigenfrequency. The right-hand panel shows the variation of the Rossby radius of deformation. Non-Doppler effects become stronger for smaller scales.

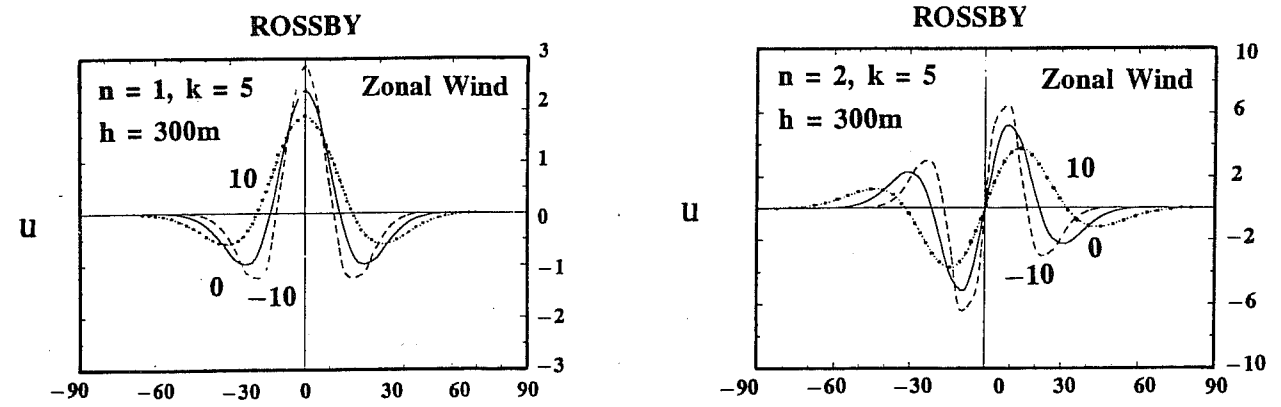

Figure 13: Structure of the n=1 (left panel) and the n=2 (right panel) k=5 Rossby modes as a function of the magnitude and sign of the basic flow. Modes within the westerly basic state are far less trapped than modes in an easterly flow. The physical reasons for the difference are given in Appendix 3 in terms of potential vorticity. From Zhang and Webster (1989).

With $U=U(y)$ the coefficients a, b, and c in *(6)* become;

$$a = \tilde{\omega}^2 - k^2 - \frac{k}{\tilde{\omega}} - \frac{U}{2} - \frac{3k^4}{\tilde{\omega}^2 - k^2}U_y^2 - \frac{k^3}{\tilde{\omega}(\tilde{\omega}^2 - k^2)}U_{yy}$$

$$b = \left(\frac{1}{2} - \frac{k^3 U}{\tilde{\omega}(\tilde{\omega}^2 - k^2)} - \frac{2k^2}{\tilde{\omega}^2 - k^2}\right)U_y y \qquad (10)$$

$$c = \left(1 + \frac{kU}{\tilde{\omega}} + \frac{U^2}{4}\right)y^2$$

Γ^2 takes on the full form indicated in *(4)*. Thus, with $U=U(y)$, the second non-Doppler term $v\frac{dU}{dy}$ of *(2)* enters the basic set of equations. Following Boyd (1980, 1983), the system can be rendered into a standard eigenvalue problem (Zhang and Webster, 1989).

Figure 14 shows the structure of the n=1, k=5 Rossby wave zonal wind structure for the two shear profiles *EE* and *EW*. Near the equator, the structure of both modes is very similar to the constant westerly basic state and both modes are less trapped in the region than the stationary basic state. Further away from the equator larger differences are observed. Poleward of about 15° the EW mode becomes significantly less trapped than the EE mode.

(iii) Longitudinally and Vertically Varying Flows: $U=U(x,z)$

Figure 10 showed that the basic state had considerable longitudinal and vertical structure with magnitudes of variation similar to the extratropics (Webster, 1983, Webster and Chang, 1988). Furthermore, the vertical shear is considerable. Clearly, there is an obvious need to assess the importance of these features of the basic flow on the structure and behavior of transients.

To procede we need to adopt a different approach. The basic equations are not separable for an arbitrary basic state. To overcome these restrictions on analytical studies, we consider a fully stratified system in a resting atmosphere. To ensure separability, we set $U=0$ renders the set separable and then calculate both vertical and horizontal group speeds (C_{gx} and C_{gy}) of the modes. Using the approximate ray tracing theory of Lighthill (1978) an analytical solution can be obtained in a local frame of reference that moves with the speed of a local flow at each point. Invariants on frequency or wavenumber can be obtained from the kinematic theory of a wave based on the characteristics of the basic flow. With these invariants, we can relate solutions at different locations and to describe the wave over the space. The first step is to obtain the local solutions.

(a) Solutions:

We assume a motionless basic state in a frame of reference that moves with a local flow. To accommodate a resting atmosphere, the basic state thermodynamic variables in the local frame must depend on height only. We assume that the basic state pressure is hydrostatic. On an equatorial β–plane, the linearized perturbational momentum, hydrostatic, mass continuity and thermodynamic equations can be written as:

$$\begin{aligned}
\frac{\partial u}{\partial t} - \beta y v &= -\frac{1}{\rho_0}\frac{\partial p}{\partial x} \\
\frac{\partial v}{\partial t} + \beta y u &= -\frac{1}{\rho_0}\frac{\partial p}{\partial y} \\
\frac{\partial p}{\partial z} &= -\rho g \\
\frac{\partial \rho}{\partial t} + w\frac{d\rho_0}{dz} + \rho_0\left(\frac{\partial u}{\partial x} + \frac{\partial v}{\partial y} + \frac{\partial w}{\partial z}\right) &= 0 \\
\frac{\partial p}{\partial t} + w\frac{dp_0}{dz} = \gamma R T_0\left(\frac{\partial \rho}{\partial t} + w\frac{d\rho_0}{dz}\right) &+ (\gamma - 1)\rho_0 J
\end{aligned} \tag{11}$$

in which ρ_0, p_0 and T_0 are the density, pressure and temperature of a basic state. u, v and w represent perturbational longitudinal (zonal), latitudinal and vertical velocities. ρ and p are perturbational density and pressure. The constant g represents the acceleration due to gravity, R the universal gas constant, and γ the ratio of specific heats. J is the heating per unit time per unit mass.

Following the procedures outlined in Appendix 3, we form horizontal and vertical equations based on the separability assumption:

$$\hat{v} = \sum V_n(z)\Psi_n(y) \tag{12}$$

where $V_n(z)$ and $\Psi_n(y)$ represent vertical and latitudinal structures of $\hat{v}$ separately. h_n represents a separation constant, $H = \frac{RT_0(z)}{g}$ the scale height of the basic state, $\epsilon(z) = \frac{dH}{dz}$, and $\kappa = \frac{\gamma-1}{\gamma}$. The horizontal equation is:

$$\frac{d^2\Psi_n}{dy^2} + \left(\frac{\omega^2}{gh_n} - k^2 + \frac{k}{\omega}\beta - \frac{\beta^2}{gh_n}y^2\right)\Psi_n = 0. \tag{13}$$

Thus, *(13)* is the same as *(6)* of Webster and Chang (1988) if we assume $c^2 = \sqrt{gh_n}$.

For an isothermal atmosphere, the vertical structure equation *(A3.3)* can be written as (Lindzen, 1967):

$$\frac{d^2V_n}{dz^2} + \left(\frac{\kappa}{Hh_n} - \frac{1}{4H}\right)V_n = -\frac{\kappa^2}{H}S_n. \tag{14}$$

Away from the source area S_n=0 and *(14)* becomes:

$$\frac{d^2V_n}{dz^2} + m^2V_n = 0 \tag{15}$$

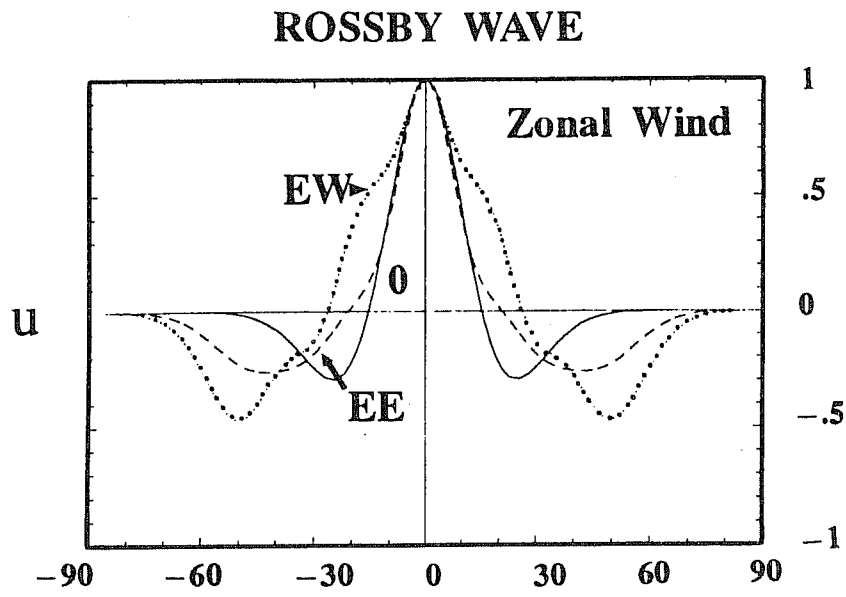

Figure 14: Distribution of the zonal velocity component of the n=1, k=-5 mode in the EE and EW basic states from Fig. 10. The structure of the mode in a resting atmosphere is shown as the solid line.

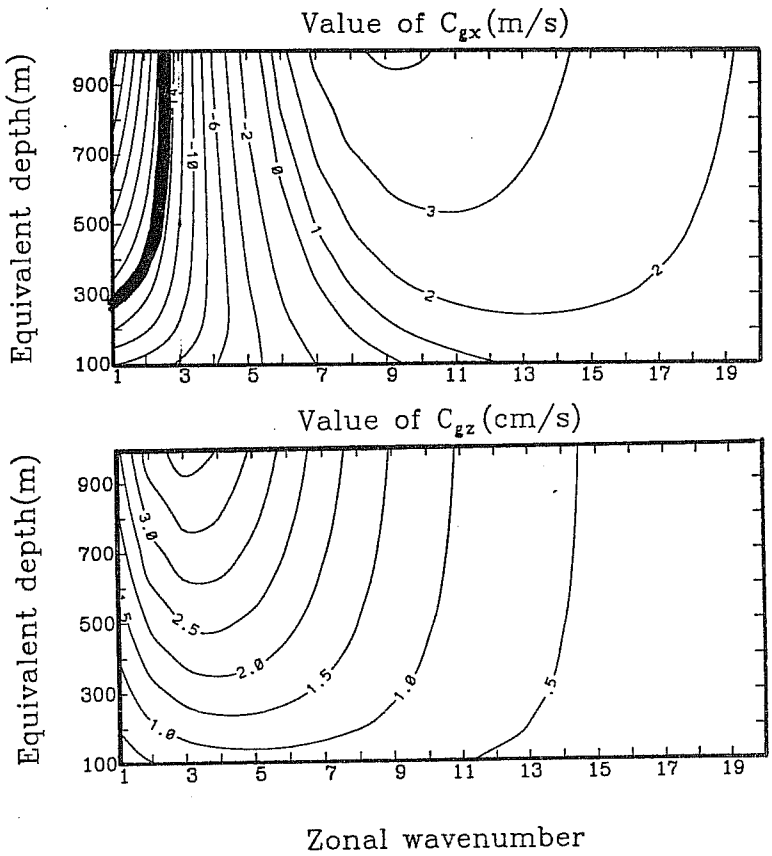

Figure 15: Distribution of the longitudinal group speed (C_{gx}, ms^{-1}, upper panel) and the vertical group speed (C_{gz}, cms^{-1}, lower panel) as a function of equivalent depth (h_n, m) and zonal wavenumber (k). To the right of the C_{gx} = 16 ms^{-1} isotach (darkened) the magnitude of the group speed component may match the magnitude of the westerly winds in the tropical upper troposphere.

where the vertical wavenumber m is defined as:

$$m^2 = \left(\frac{\kappa}{Hh_n} - \frac{1}{4H^2}\right). \tag{16}$$

Combining *(15)* and *(16)*, we have a dispersion relation:

$$\omega = -\frac{\beta k}{\left[k^2 + \frac{\beta}{N}(2n+1)\left(m^2 + \frac{1}{4H^2}\right)^{(1/2)}\right]} \tag{17}$$

where $N^2 = \frac{g\kappa}{H}$ with n representing the latitudinal node number.

(b) Horizontal and vertical group speeds:

From *(17)*, we can obtain zonal and vertical group velocities as

$$C_{gx} = \frac{\partial \omega}{\partial k} = \frac{\beta\left[k^2 - (2n+1)\frac{\beta}{N}\left(m^2 + \frac{1}{4H^2}\right)^{(1/2)}\right]}{\left[k^2 + (2n+1)\frac{\beta}{N}\left(m^2 + \frac{1}{4H^2}\right)^{(1/2)}\right]^2} \tag{18}$$

and

$$C_{gz} = \frac{\partial \omega}{\partial m} = \frac{(2n+1)\frac{\beta^2 k}{N}\frac{m}{\left(m^2+\frac{1}{4H^2}\right)^{(1/2)}}}{\left[k^2 + (2n+1)\frac{\beta}{N}\left(m^2 + \frac{1}{4H^2}\right)^{(1/2)}\right]^2} \tag{19}$$

Figure 15a shows values of C_{gx} for different values of zonal wavenumbers and equivalent depths. Here, the abscissa is zonal wavenumber k. The ordinate is h_n which can be related to vertical wavenumber m through *(16)*. A large/small value of h_n corresponds to a small/large value of m, i.e., a deep/shallow Rossby wave. For example, if we set $T_0 = 250^o K$, then $h_n = 100m$ corresponds to a wave 10.12 km deep, $h_n = 200m$ to 14.5 km, $h_n = 500m$ to 23.19 km, and so on. Thus, for the range of h_n discussed here, the speeds of westward moving Rossby waves decrease monotonically as the values of k increases. For eastward moving Rossby waves, there is a maximum speed located between k = 9 and 14. Variations of h_n (i.e., vertical wavenumber m) also modify the values of C_{gx}, especially for long and shallow waves (i.e., small k and h_n). In the range of $3 \leq k \leq 6$ and 300m $\leq h_n \leq$ 1000 m, the value of C_{gx} is almost independent of h_n. For very short waves (k $\geq$ 11), C_{gx} depends more greatly on h_n than k. Figure 15b shows the distribution of C_{gz} for different values of k and h_n. For the simple atmosphere used here, the Rossby wave vertical group velocities are always upward and both k and $h_n$are very important in determining the values of C_{gz}.

(c) Rays:

From kinematic wave theory, we know that if a background wind field varies in space very gradually, then the relationship between the frequency ω_d in a frame that is fixed in space and the frequency ω in a frame that moves with the same speed as a local wind can

be obtained simply. If the background wind field only has a zonal component $U(x,z)$, then the relationship can be written as

$$\omega_d = \omega + Uk \tag{20}$$

where ω is the same as defined by *(17)*. If we follow a wave with its local group velocity, we can draw a ray in space. Equations that describe the ray are (Lighthill, 1978):

$$\frac{dx}{dt} = \frac{\partial \omega_d}{\partial k} = U(x,z) + C_{gx}, \tag{21}$$

$$\frac{dk}{dt} = -k\frac{\partial U}{\partial x}, \tag{22}$$

$$\frac{dz}{dt} = \frac{\partial \omega_d}{\partial m} = C_{gz}, \tag{23}$$

$$\frac{dm}{dt} = -k\frac{\partial U}{\partial z} \tag{24}$$

where $\frac{d}{dt}$ represents the derivative following a local group velocity.

(d) Rays in the longitudinal plane:

If we return to Fig. 10 we can obtain an estimate of the magnitude of the mean zonal flow in the equatorial belt. In the upper troposphere the magnitude varies from about +15 ms^{-1} to about –12 ms^{-1}. If we compare this velocity range with the zonal group speeds shown in Fig. 15a it appears that there is the possibility for modes to possess zero longitudinal Doppler group speeds over a wide scale range. The region to the right of the – 16 ms^{-1} group speed isotach (heavy solid line) defines the modes that potentially possess zero Doppler-shifted group speeds. However, from *(22)*, a mode may change its scale (and, therefore, its group speed from *18*) if U changes along the ray. The diagram indicates, too, that nearly all modes are candidates for considerable modification of their scale and group speeds.

The importance of this modification is that a slowing of the group speed of a mode indicates that their would be a convergence of wave energy flux into a particular region. Whitham (1965) and Bretherton and Garrett (1968) showed that wave action flux is conserved along a ray. In terms of the energy density of a wave, Δ, Webster and Chang (1988) showed that the conservation law can be written for an equatorial Rossby wave as:

$$\frac{\partial \Delta}{\partial t} + C_{gx}\frac{\partial \Delta}{\partial x} = -\frac{dU}{dx} \tag{25}$$

where $\Delta = \rho g h^2$. Thus, in region where the stretching deformation is negative (e.g., to the east of the westerly maximum) there will be a convergence of energy density. Conversely, where $U_x<0$, there will be divergence of Δ.

Using *(18)*, *(21)* and *(22)*, Webster and Chang (1988) calculated the horizontal Rossby wave propagation in a mean zonal wind field with longitudinal variation. Figure 16 shows

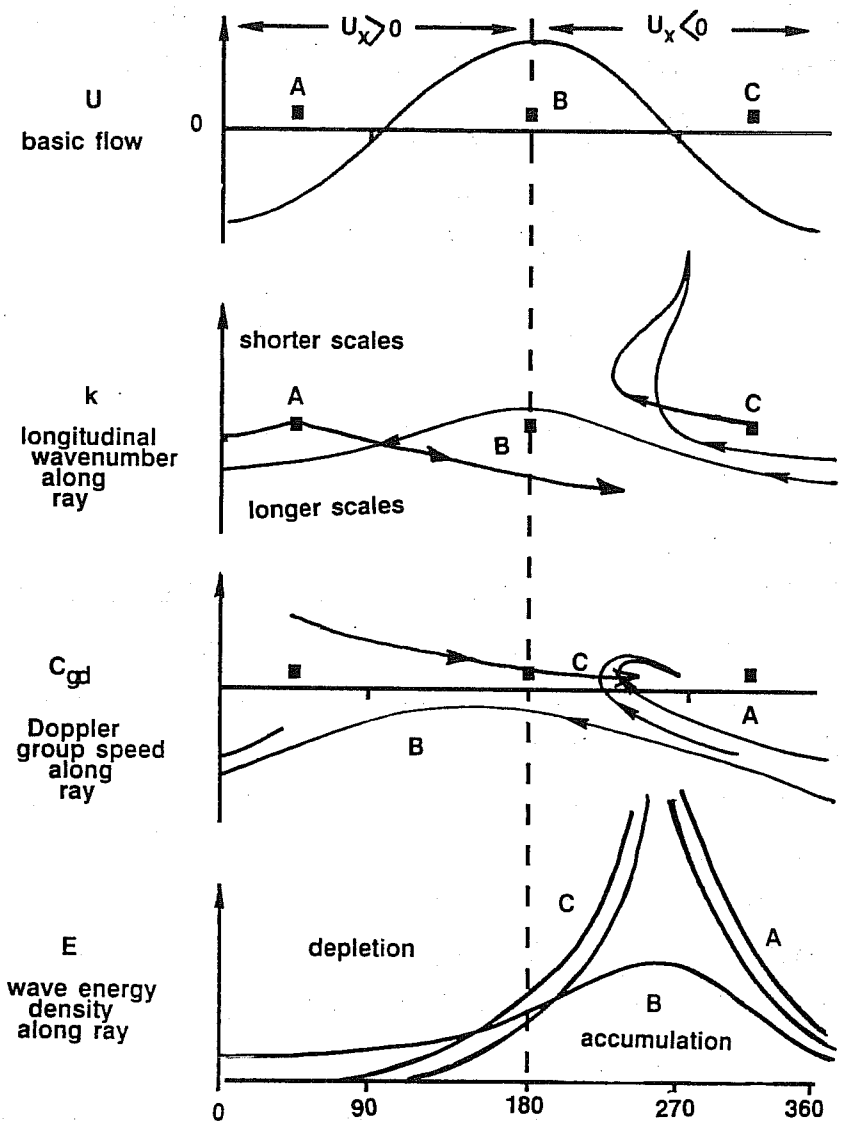

Figure 16: Schematic diagram representing the results of a WKBJ analysis for equatorially trapped Rossby waves in a basic flow with longitudinal stretching deformation (upper panel). Wave sources are located at A, B, and C. Second panel shows the variation of the wavenumber along the ray as given by *(22)*. Depending on whether the waves are short or long, they will move westward or eastward where their longitudinal scale contracts or extends, respectively. The final effect is that the Doppler shift of all modes (except the very longest) will approach zero in the vicinity of where the negative stretching deformation is a maximum as indicated in Fig. 6 and 7. In the region where $C_{gxd} \rightarrow 0$, wave energy density will accumulate as suggested by *(25)*. From Webster and Chang (1988).

an example of the horizontal ray paths for a simple sinusoidal basic state with a 10 ms^{-1} amplitude. There are a number of points to note. All modes tend to "accumulate" in regions where the stretching deformation is negative. Also, irrespective of where the mode originates, the region of accumulation is the same. But not all modes accumulate from the east. Shorter waves may accumulate from the west. For convenience, we refer to the two forms of accumulation as "forward" and "backward" accumulation.

Fig. 17a shows a schematic diagram of the "forward" and "backward" accumulation. For a given value of the equivalent depth that there is a particular wavelength at which the zonal group velocity changes sign (Fig. 15a). For $h_n < 300$ m the transition occurs between $k = 7$–9. Thus, if we imagine an episodic forcing occuring which takes place (say) in the warm pool regions of the tropical Pacific Ocean, we might imagine that, initially, a short wave packet will move eastward while a long wave packet will move westward. The long wave packet will eventually move into a region of negative stretching deformation. From *(22)* k must then increase so that the group velocity tends towards zero. On the other hand, the short wave packet will move into a region of positive stretching deformation so that k must decrease. Thus, for the short packet also, the group velocity will tend to zero. Therefore, *both wave packets accumulate in the vicinity of the westerly maximum.* Also, as each packet moves into the region of westerlies, we would expect that the modes will tend to extend poleward as the modes become less trapped (see section 3.4a). Figure 17b summarizes the changes in lateral scale as a function of longitudinal wavenumber for the short and long wave packets. The diagram shows the change in modal turning latitude for the long wave packet (dashed line A-B) as it moves westward from the easterly to westerly regime. The solid line (C-D) shows the change in turning latitude for the short wave packet as it makes the same regime change but in the opposite direction.

It should be noted that we have not discussed the accumulation properties of the mixed Rossby-gravity mode. Given that this mode possesses an eastward group speed for all scales, it will accumulate in the negative sense. It would seem, then, that modes of the scale studied by Liebmann and Hendon (1990) (i.e., $k>8$) may be of some significance in accumulation in the mid-ocean trough regions and, thus, on the extratropics immediately poleward of the region. Long mixed Rossby-gravity modes would have very large positive group speeds which may not be effected too much by the stretching deformation of the zonal flow.

(e) Rays in the longitude–height plane:

Equation *(24)* indicates that if the zonal wind field contains a vertical shear, then m will be changed along a ray. Thus, a reasonable question might be whether or not the transient modes may propagate out of the troposphere before they approach the accumulation regions.

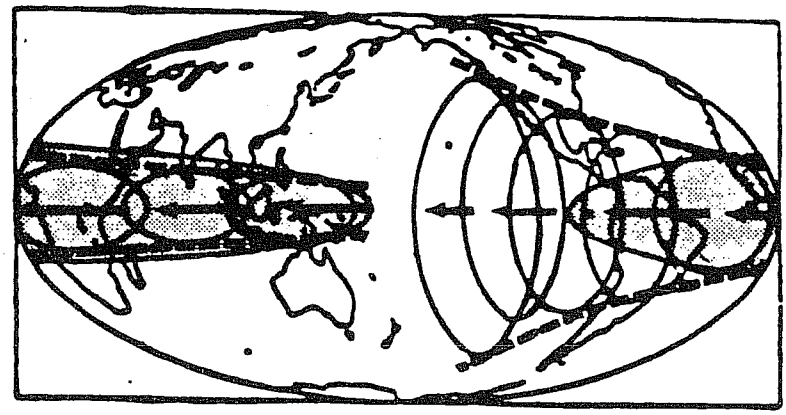

FORWARD ACCUMULATION

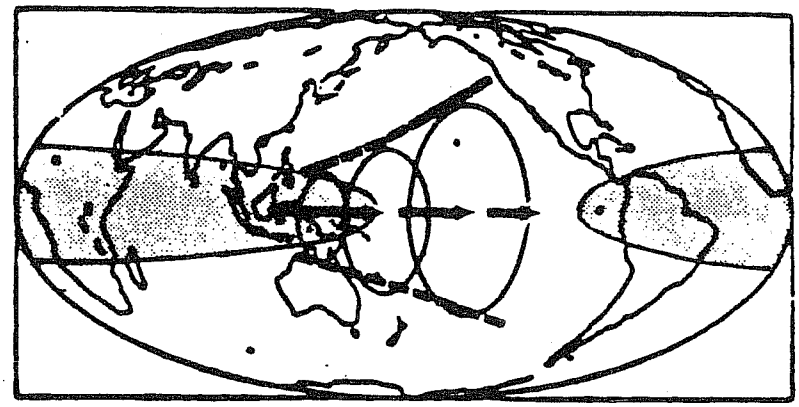

BACKWARD ACCUMULATION

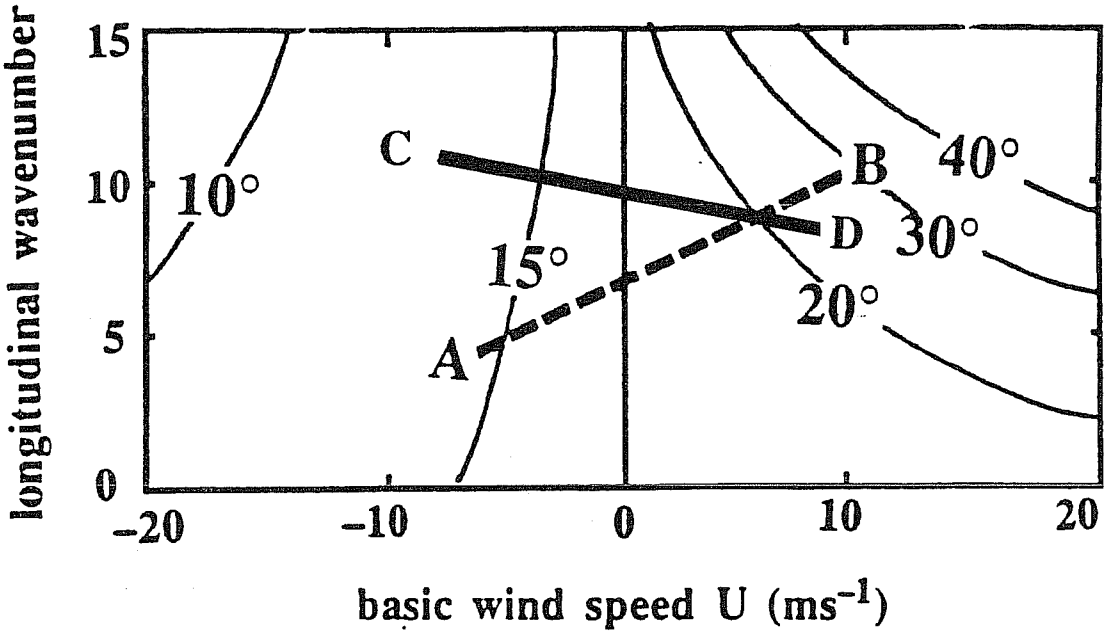

Figure 17: (a) Schematic representation of the "forward" (upper panel) and "backward" (lower panel) accumulation processes for the long and short wave packets. The region of accumulation is also where the modes will "swell" to higher latitudes (see Figs. 13 and 14). (b) Contours of the turning latitude of the n=1 mode as a function of longitudinal wavenumber and the basic wind speed. The dashed line (*A-B*) indicates the variation of the turning latitude and scale of a long wave packet mode propagating westward. The solid line (*C-D*) indicates the variation of the short wave packet propagating eastward away from the source region. From Chang and Webster (1990).

Also, *(24)* shows that m will change along a ray depending on the sign of the vertical shear. From *(16)* we can see that if m changes then h_n will change, which, from Fig. 15b, can alter k and thus the horizontal group velocity C_{gx}. These associations are the reasons why we need to reexamine the results of Webster and Chang (1988) in a $U(x,z)$ basic state.

Figure 18 presents a schematic version of the influence of a basic state $U(x,z)$ on the modal structure. Noting the inverse relationship between m and h_n from (16), which may be approximated as:

$$m^2 \approx \frac{\kappa}{h_n}, \qquad (26)$$

so that $h_n \propto L_z$, insists that the vertical scale goes as the equivalent depth. Then, from *(24)*, if $U_z<0$, the vertical scale decreases (i.e., m increases). But if $U_z>0$, the vertical scale decreases (i.e., m decreases). Figure 18a represents *(24)* and shows the change of vertical scale for a mode propagating through negative and positive shear regions. Figure 18b describes *(22)*.

With the relationships between m and U_z established, we can consider the interdependency of the vertical and horizontal properties of the modes. Figure 18c shows the mode trajectories in (k-m) space for arbitrary variations along a ray in a $U(x,z)$ flow. The arrows indicate mode characteristic trajectories for different combinations of stretching deformation and vertical shear. The letters (A, B, C and D) denote the possible shear-stretching combinations which define unique variations of m and k of a mode propagating through an arbitrary $U(x,z)$. The letters are also marked on the lower panel which shows a cross-section of $U(x,z)$ along the equator. Suppose a transient wave is forced in the low level easterlies of the tropics (i.e., a location which would correspond to the convectively active warm pool region of the western Pacific Ocean). Short and long wave packets would emerge from the region. The long wave packet will be confined to the troposphere where $U_z< 0$ (D and C) but will extend rapidly into the stratosphere in the region of positive shear near the mid-ocean troughs (A and B). The short wave packet, on the other hand, would also be constrained to the troposphere (region C) during its shorter eastward propagation before arriving at A where it will also rapidly propagate in the vertical in the vicinity of the mid-ocean trough. From Section 3.4(i) we recall that in the same locations (A and B), the modes will also expand in latitude.

Figure 19 shows rays of Rossby waves in an x-z plane for different values of k and h_n with n=1. The integration period is 15 days which is the time required for a Rossby wave to travel horizontally from an energy source to an accumulation region (Chang and Webster, 1990). The figure indicates that in the absence of a basic wind field, Rossby waves can penetrate up to 35 km height. Deeper waves (larger value of h_n) will propagate higher than will shorter waves. The wave with a zonal wavenumber near k = 5 has the largest vertical group velocity.

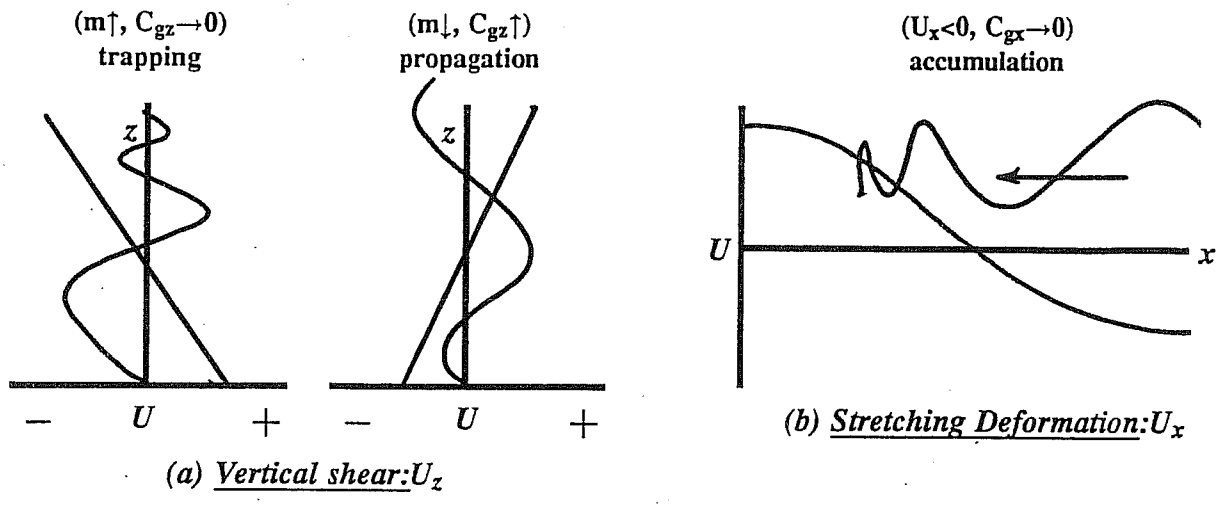

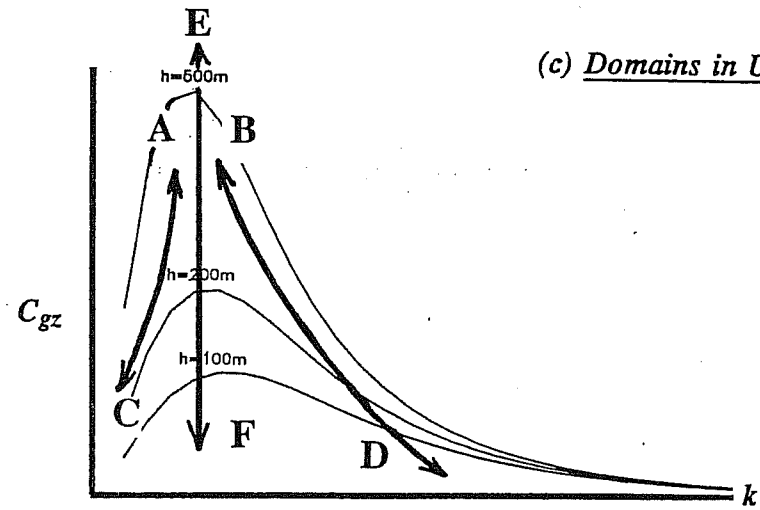

(c) Domains in U(x,z)

	U_z	U_x	m	k	X	Z
A	+	+	↓	↑	Prop	Prop
B	+	−	↓	↓	Accm	Prop
C	−	+	↑	↓	Prop	Trap
D	−	−	↑	↑	Accm	Trap
E	+	0	↓	-	-	Prop
F	−	0	↑	-	-	Trap

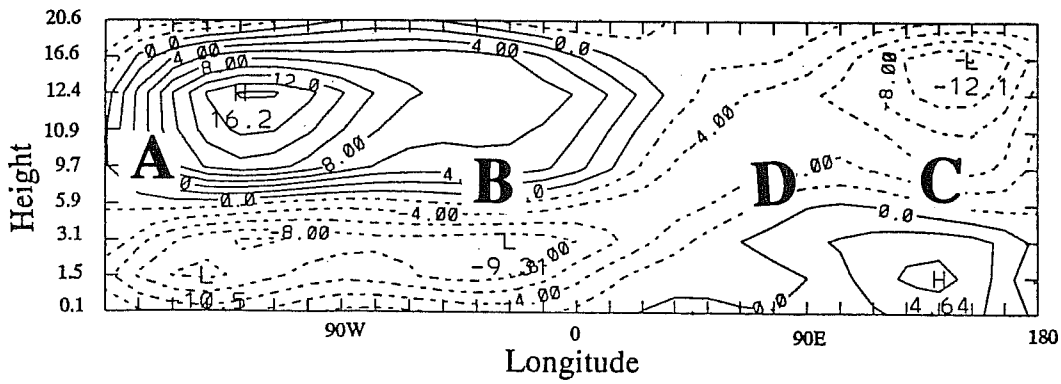

Figure 18: Schematic diagram interpreting *(21)-(24)* in an arbitrary *U(x,z)*. (a) For $U_z<0$, the vertical wavenumber, *m*, increases (wavelength decreases) and $C_{gz}\rightarrow 0$ indicating a vertical trapping of the mode. With $U_z>0$, *m* decreases so that C_{gz} increases and the mode may propagate upwards more rapidly. (b) If $U_x<0$, *k* increases and $C_{gx}\rightarrow 0$ and the mode is longitudinally trapped (accumulation) and . If $U_x>0$, *k* decreases and C_{gx} becomes larger as shown in Fig. 16.. (c) $C_{gz}(k)$ for various h_n. Four regimes are possible (A, B, C and D). E and F occur when $U_x=0$. The arrows indicate the "trajectory" of the rays in *(m,k)*-space and is summarized in the table for long waves.The lower diagram shows the regions where the modal modifications will take place. In summary, near the mid-ocean troughs (e.g., regions A-B) modes will accumulate longitudinally while extending both vertically and latitudinally.

Before examining the full impact of a $U(x,z)$ flow, we will examine *(23)* and *(24)* with a basic wind field that varies in the z direction only. Figure 20a shows the vertically distribution of the zonally averaged U-field for the long term average between 1958–88 (heavy solid line) and two phases of Quasi-biennal Oscillation (QBO); the easterly (solid) and the westerly (dashed) descending phases (e.g., Maruyama, 1967). Figure 20b displays rays of Rossby waves in an (x-z) plane relative to the wind profile shown on the left-hand side of the diagram and is similar to the profile used by Maruyama (1967). It is obvious that shorter waves have experienced larger modifications which is consistent with *(24)*. Toward the end of the 15–day integration period, the vertical group velocities, C_{gz}, of the k=4, 5 and 6 waves become very large so that these waves would certainly propagate out of the troposphere if the integration were continued beyond the 15 days.

The waves in the motionless basic and the easterly descending basic states (Figs. 19 and 20b) travel to nearly the same heights at the end of the integration. The $U(z)$ profile to the left of Fig. 20a shows that the waves in the easterly descending basic state must experience a vertically negative shear area before they are exposed to the upper troposphere lower stratosphere positive shear region. At the end of the integration period, modifications of vertical group velocity by the negative and the positive shears are almost the same.

Figure 20b depicts Rossby wave rays propagating through the westerly descending phase of a QBO period. Compared to the easterly descending phase, the waves do not propagate as far in the horizontal but more in the vertical than either the westerly descending case or when there is a zero-basic. The longer horizontal travel of Rossby waves in the westerly descending basic state is because of the larger tropospheric mean easterly wind. The large negative shear in the upper troposphere to the lower stratosphere of the westerly descending basic state (Fig. 20b) certainly limits the wave's vertical propagation at the end of the integration period. Thus, a Rossby wave can reach only the lower stratosphere during a westerly descending phase of a QBO period.

Figure 21 provides a smoothed version of the mean 1978–85 December zonal wind field in which only Fourier components $k \leq 3$ are included.[12] To apply the ray tracing theory to this more complicated case, we assume that the spacial scales of a background wind are much larger than that of the waves we want to trace. For the basic state shown in the Fig. 21, the longest wave must have a zonal wavenumber $k \geq 4$. To obtain the proper equivalent depth h_n, we rearrange *(13)* as:

$$\sqrt{gh_n} = \frac{a\Omega(2n+1)}{k^2\left(\frac{2\Omega}{\omega k}-1\right)}\left[1+\sqrt{1-\left(\frac{\omega}{\Omega}\right)^2\left(\frac{k}{2n+1}\right)^2\left(\frac{2\Omega}{\omega k}-1\right)}\right] \qquad (27)$$

[12] The data were obtained from the Climate Diagnostic Data Base (CDDB) and prepared by the Climate Diagnostic centre of the National Meteorological centre (NMC).

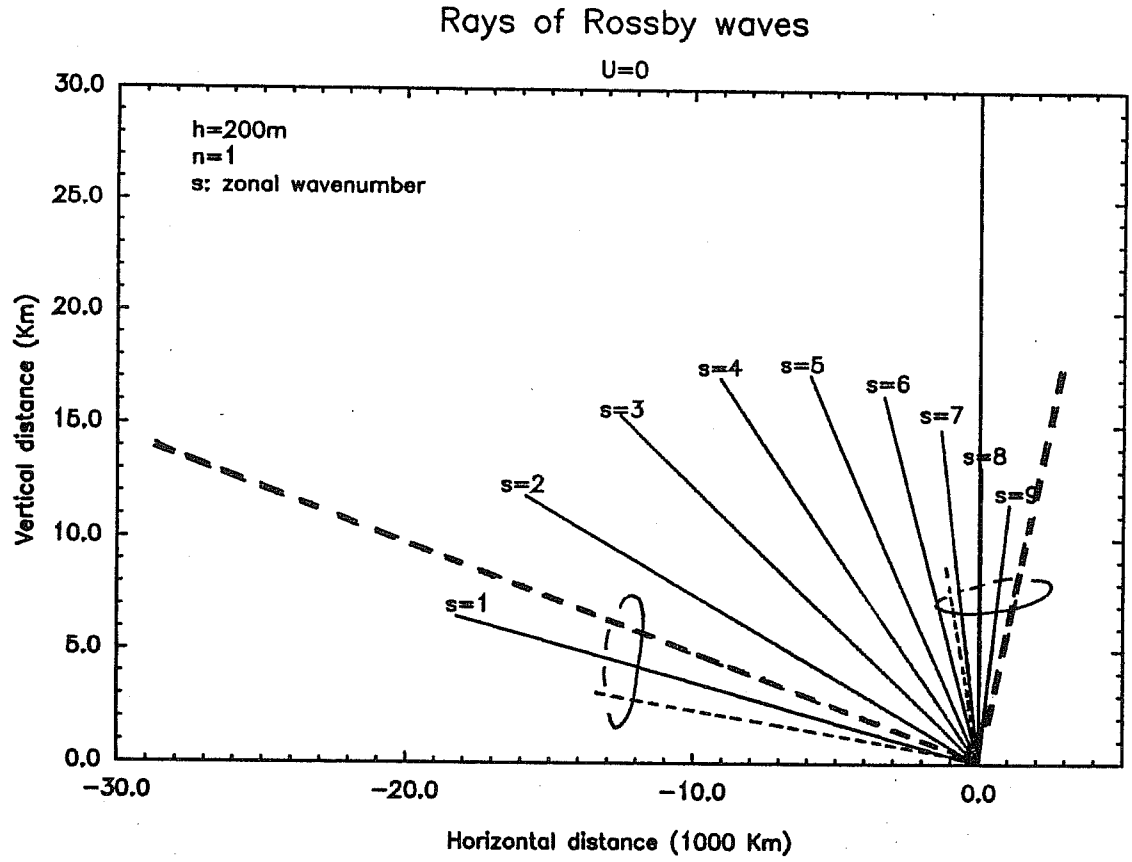

Figure 19: Rays in the (x,z) plane in a resting atmosphere of the n=1 Rossby mode for different longitudinal wavenumbers. Lines indicate the ray trajectory over a 15 day period. Solid lines show rays for h_n=200 m. Curves for h_n= 500 m (dashed) and 100 m are shown for k=1 and 9 as dashed and dotted lines, respectively. From Webster and Chang, 1991.

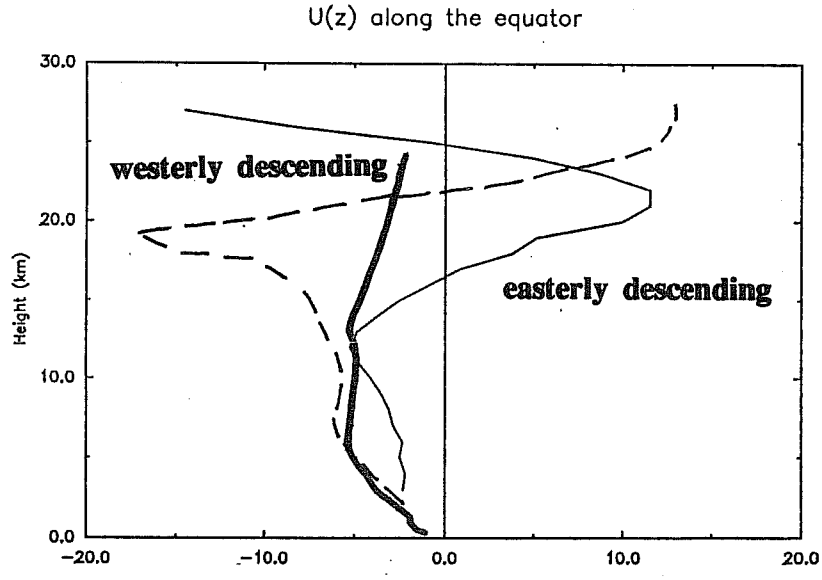

Figure 20a: Zonally averaged U profiles along the equator for the long term average (1958–1963; heavy solid curve), the westerly descending phase of the QBO (March-April, 1963; dashed line) and the easterly descending phase (July-August; solid curve). Data from Newell, *et al*, (1974). From Webster and Chang, 1991.

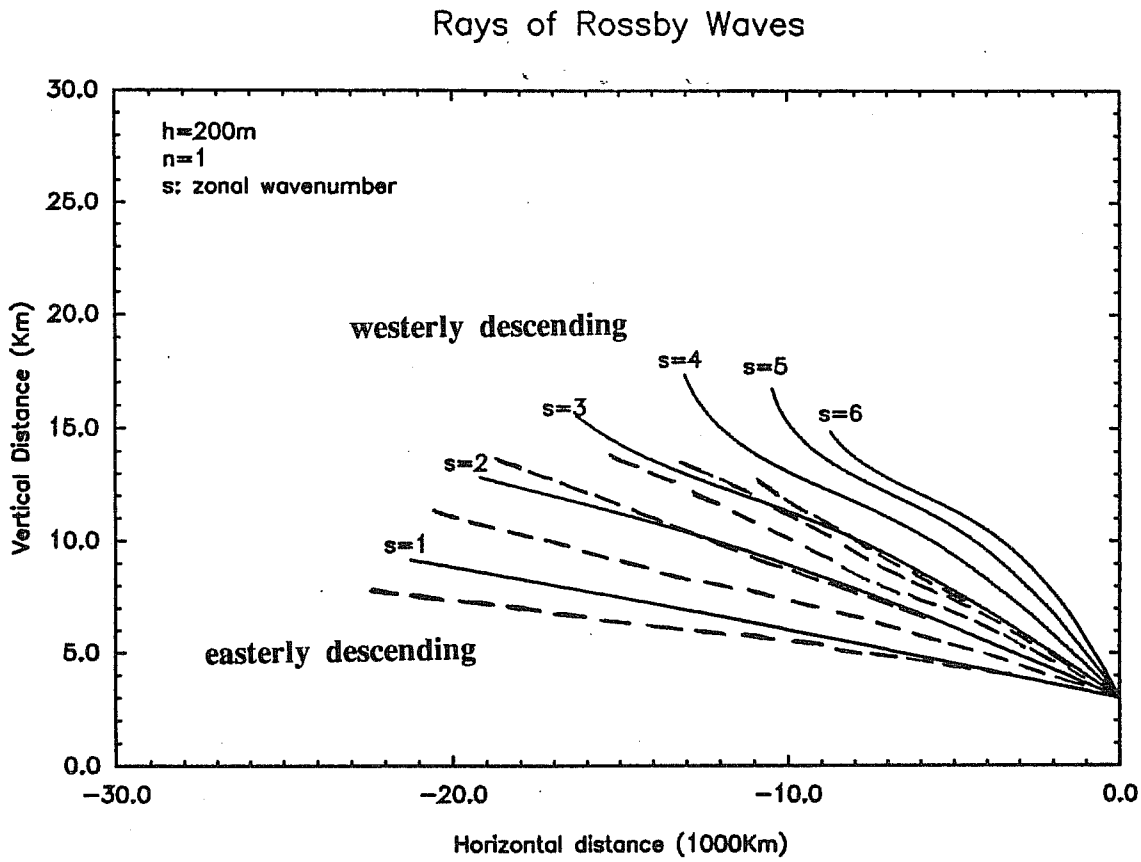

Figure 20 b: Rays in the (x,z) plane for the Rossby n=1 mode in a 200m equivalent depth fluid. Solid lines denote rays associated with the westerly descending phase; dashed curves denote rays with the easterly descending phase. From Webster and Chang, 1991.

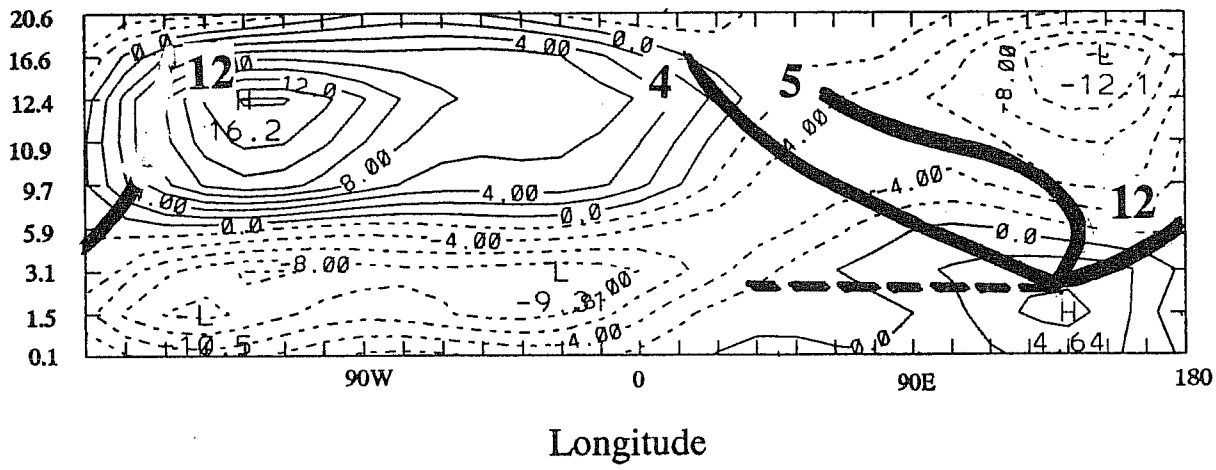

Figure 21: Smoothed version (k=0, 1, 2, 3 and 4) of the vertical cross-section of the zonal winds shown in Fig. 10. Heavy curves denote the rays of the k=4, 5 and 12 Rossby waves.

where Ω is the angular speed of rotation of the earth. If we know the initial wavenumber k, angular frequency ω and latitudinal node n of a wave, we can obtain h_n from (23). For a wave with initial k=4, n = 1 and ω=2π/(10days), the value of h_n is 197m; the corresponding vertical wavelength is approximately 14 km. Solving *(21)* – *(24)* gives the ray which is superimposed on Fig. 21. The starting point of the tracing is 120°E and 3 km height. After a relatively rapid westward propagation, the mode reduces its westward propagation speed and increases its vertical movement. After a 10 days of integration, the wave has reached 31°E and 16 km height. Rays for shorter waves are also plotted on Fig. 21. The k=5 mode moves less westward. However, the k=12 wave, representative of the short wave packet, moves eastward and rapidly upward in the equatorial westerlies.

To separate out the impact of basic wind vertical shear and Rossby wave vertical propagation on the energy accumulation theory from the horizontal effects, we consider the impact of the horizontal stretching deformation separately. Using only *(21)* and *(22)*, and assuming that the 200 mb flow is representative of the zonal flow, the horizontal ray trace can be computed. The temporal variation of the ray is shown as the heavy dashed line in Fig. 21. The farthest the wave propagates is to around 46°E, which is about 15° to the east of the wave that is effected by both the horizontal and vertical variability of the basic state.

To explain the differences between the various components of the background flow, we must realize that along the rays of the two waves different parts of the mean flow are experienced by each wave. In this way, each wave experiences totally different advecting and stretching regimes although the overall basic wind field is the same. When the vertical variations of the basic state are ignored, the wave experiences a relatively uniform strong negative stretching effect during the entire integration period. For U_x constant, *(22)* shows that the k increases exponentially with time. Figure 15a indicates that C_{gx} should decrease exponentially in the early stages of the integration when the wave has a westward group velocity and remain relatively uniform when C_{gx} becomes positive. In the early stages of the integration, the background wind decreases linearly with time and C_{gx} decreases exponentially with time. Toward the end of the integration period, k becomes very large and the C_{gx} becomes positive. The wave still moves westward with a speed decreasing with time, because the background wind still has a negative value that is larger than the value of C_{gx}.

The situation for the wave that propagates in both horizontal and vertical is very different. Given the location of the wave source, the wave first experiences a westerly flow in the lower troposphere. Thus, the wave can only propagate vertically during this time. After the ray moves above the 6 km level, a relatively horizontally uniform easterly wind field appears. During this stage, the wave moves very rapidly to the west because both the background wind and the zonal group velocity C_{gx} have large negative values. After the ray reaches

45°E and 11 km height , it experiences a strong negative horizontal stretching and positive vertical shearing effects. From *(23)* and *(24)*, we know that k will start to increase and m will start to decrease. In fact, the value of C_{gx} will become small and the value of C_{gz} will become large. In addition, the magnitude of the background wind also becomes very small in this region and the wave begins decelerating in the horizontal and accelerating in the vertical. Most of the differences in the ray paths in the *U(x)* and *U(x,z)* cases result from the persistently stronger stretching deformation encountered by the wave in the former case.

(iv) Shear Flows With Deformation: *U=U(x,y)*

Experiments using a full variability of the basic state (i.e., *U(x,y,z)*) fall into the realm of a general circulation model study. But, as one further intermediate step prior to the use of general circulation models, we can consider the impacts of basic states in which the flow varies in longitude and latitude (i.e., *U(x,y)*) noting the impact of the vertical propagation. That is, where the mode is most vertically trapped in the convective regions of the tropics (i.e., $U_z < 0$), the mode is most equatorially trapped. Only in the regions of positive vertical shear, which coincide with regions of horizontal accumulation, is the vertical mode free to propagate. Thus, the possibility of vertical escape of a mode to the stratosphere before it reaches the region of accumulation is reduced. Additionally, the confinement of the transient wave in the upper troposphere as it moves away from the source region, gives some credence to the use of the upper tropospheric flow as representative of the tropics as used by Webster and Chang (1988) and Chang and Webster (1990). But, we note as well, though, that the total horizontal propagation is different when the vertical propagation is not ignored. With these caveats and remarks in mind, we can obtain some indication of the impact of the seasonal (or epochal) impact of the basic state on the propagation of transients.

Figure 22 shows the longitudinal stretching deformation along the equator for the long term average boreal winter and summer and for the boreal winter during El Niño and La Niña periods. The periods of strongest stretching deformation occur during DJF during "normal" years and the La Niña when the westerlies are strongest in the eastern Pacific Ocean. During the El Niño period the westerlies are weak in the Pacific but much stronger in the central Atlantic Ocean. The JJA profile is typical of boreal summers even during the extremes of the Southern Oscillation. At this time of the year the longitudinal gradients of the wind fields are extremely weak. Figure 23 show the corresponding longitude-time sections of the perturbation *U*-field along the equator for a period of 25 days following episodic forcing. The same two-day e-folding forcing as Webster and Chang (1988) is used. The model is a nonlinear shallow water model with a 200 m equivalent depth. In the DJF and La Niña cases there is very strong accumulation in the Pacific Ocean and weaker accumulation in

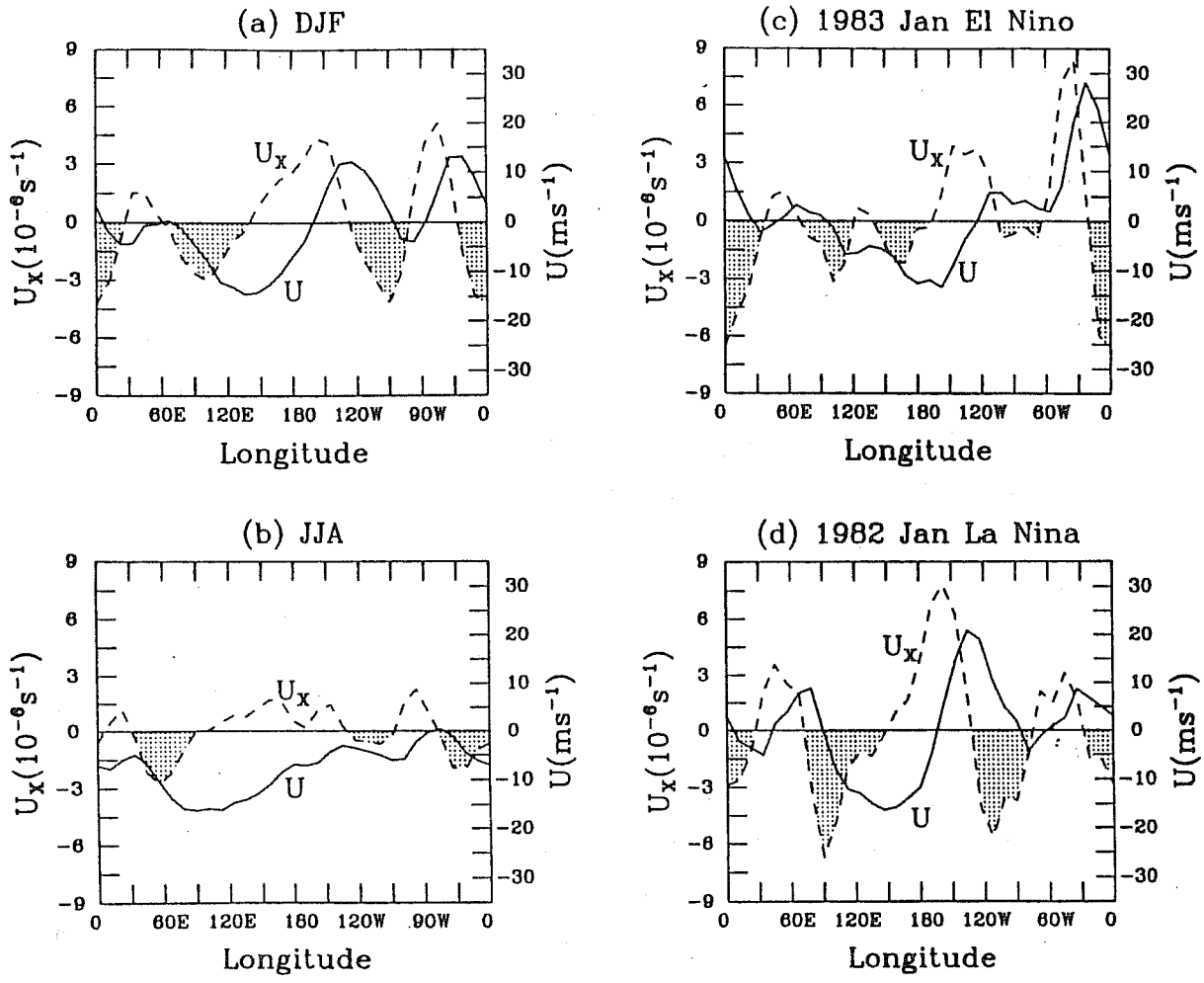

Figure 22: The zonal wind and stretching along the equator for (a) DJF, (b) JJA, (c) 1983 El Niño and (d) 1982 La Niña. Shaded areas denote negative stretching deformation. Chang and Webster (1990).

the Atlantic. During an El Niño the situation is reversed. However, during the summer (JJA) there is virtually no accumulation along the equator at all. The heavy bars indicate the regions of maximum accumulation.

Figure 23 suggests that during the year we may expect that the location or existence of an accumulation zone in the tropics to vary considerably. During winter we may expect rather strong influences from the equatorial regions in both mid-ocean trough regions but very little during the summer. During El Niño periods it would seem that the Atlantic would be the principal region of communication. However, during La Niña the region shifts to the Atlantic. Figure 24 summarizes a number of experiments where transients were forced in different, and fairly realistic, basic flows (Chang and Webster, 1991). The arrows indicate the location of the accumulation and emanation (or extension) regions that may be expected during El Niño and La Niña periods.

(v) General flows: $U(x,y,z)$

At least two studies of the accumulation/emanation phenomena have been made using full global multi-level models. The first, which used the NOAA/NMC operational model, is reported in O'Lenic, *et al.*, (1985) and Frederiksen and Webster (1986). In a number of experiments the model was perturbed in different regions by the introduction of errors into specific regions of the tropics.[13] The experiments showed that the response either in the tropics or extratropics was relatively independent of where the data transplant was made. The maximum tropical perturbation was always in the regions of upper tropospheric westerlies along the equator (i.e., the Atlantic and the Pacific) and the maximum extratropical perturbation occurred over Europe. The results were interpreted as evidence that the transient modes generated in the error source regions (i.e., where the ECMWF data was inserted) were accumulating and emanating from the mid-ocean trough regions. Gelaro (1990), using the NEPRF model found similar indications of regional activity.[14]

3.5 Reciprocity of the Interaction Between the Tropics and the Extratropics:

In the preceding paragraphs, we have emphasized the modification of transient equatorial modes in realistic basic flows and the manner in which these modes, through their

[13] The initial experiments were an attempt to ascertain the importance of "uncertainty" in the initial state in introducing errors into a forecast. As it is very difficult to determine the errors involved in a particular initial data set, the "uncertainty" was defined as the difference between two realizations of the "same" data set by two different operational centres. Thus experiments were run using the NMC initial data but with ECMWF data planted in different regions. The results were then compared to a standard run.

[14] Work is currently underway at NMC and ECMWF to perform careful experiments on the accumulation process. In order to check on the vertical propagation characteristics, discussed above, the experimental 31–level model at ECMWF is being used.

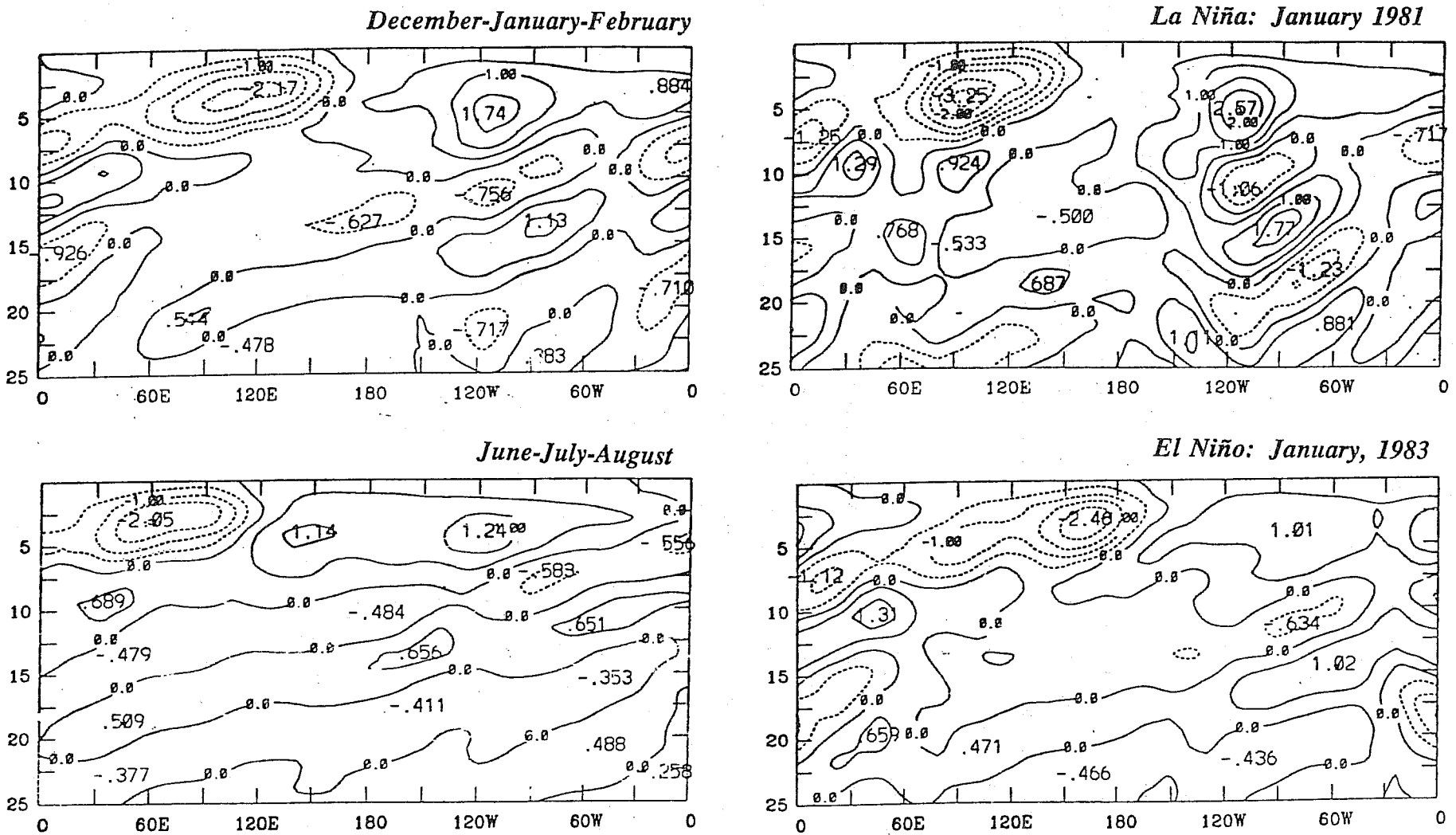

Figure 23: Time-longitude plots of the zonal velocity component around the equator for 25 days for the four basic states shown in Fig. 22. The model used is a shallow water system with realistic $U(x,y)$ basic fields.

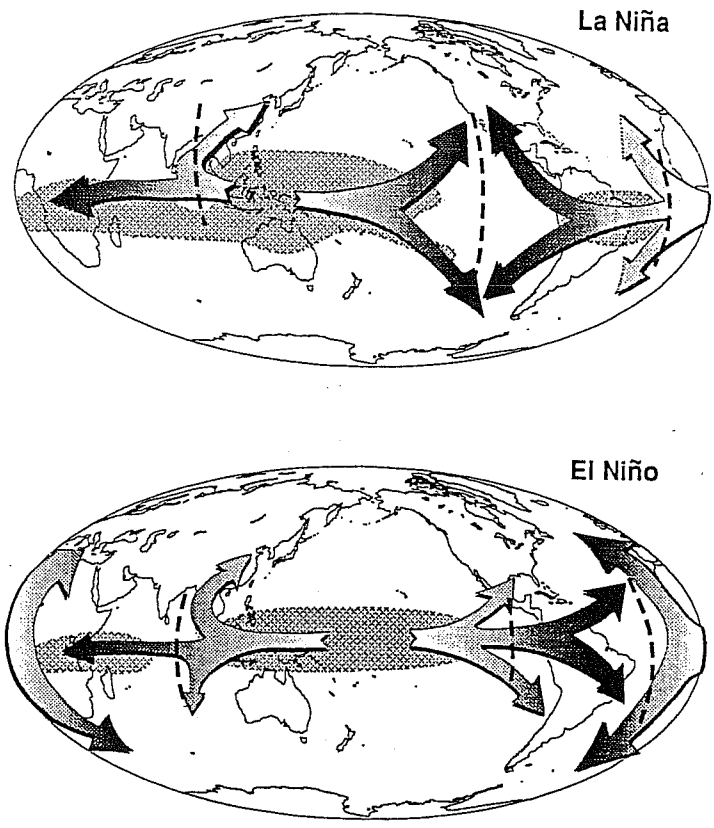

Figure 24: Schematic diagram showing the paths of equatorial transients that may be expected during extremes of the SOI. The hatched region denotes easterlies in the basic state. During El Niño the major communication between the tropics and extratropics would be in the Atlantic Ocean compared to the Pacific during La Niña. Chang and Webster (1990).

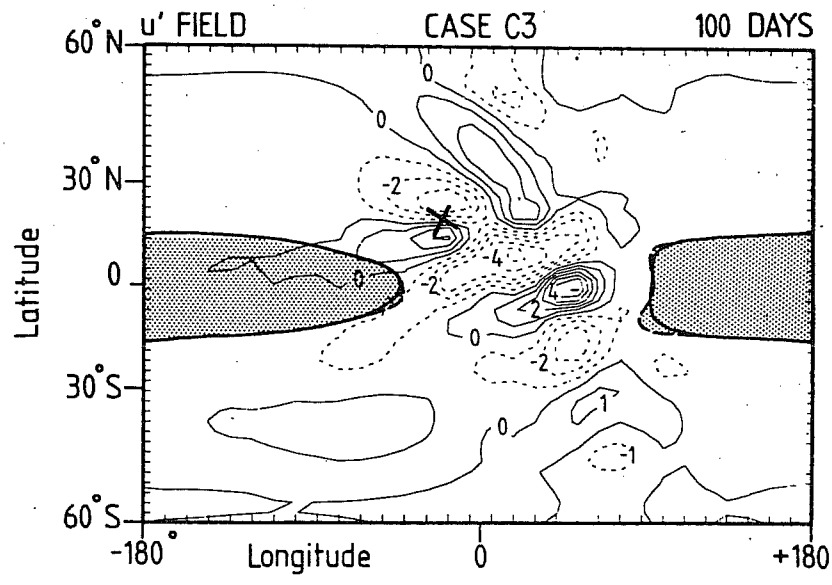

Figure 25: Propagation of extratropical disturbances into the tropics. Forcing is located at point "X" in the northern hemisphere subtropics. Field shown is the perturbation U–field. Shaded region denotes easterlies in the basic state. Wave can be seen to propagate through the "westerly duct". From Webster and Holton (1982).

modification, extend into and influence higher latitudes. Theoretical arguments have clarified observations which indicate that the influence towards the extratropics would pass through the mid-Pacific and Atlantic Ocean regions principally because they are regions of upper-tropospheric westerlies. However, an earlier study by Webster and Holton (1982) indicated that extratropical disturbances also enter the tropics, or propagate through to the other hemisphere, in these same regions. They argued that low frequency modes would not encounter a critical latitude when westerlies extend from hemisphere to hemisphere may be inferred from Fig. 10. An example of the results of Webster and Holton is shown in Fig. 25.

It seems reasonable to use the results presented in this paper to reinterpret the hypothesis of Webster and Holton. Here we have shown that, as an equatorial mode moves into the equatorial westerlies, it will extend laterally towards the poles. That is, the mode becomes less trapped. Thus, a complete set of modes would include those which would have turning latitudes which extend well into the higher latitudes. If we now imagine that some form of transient forcing develops in the North Pacific Ocean to the north of the equatorial westerlies, then, from a formalistic perspective, the forcing could project onto an extended equatorial mode. In this manner, extratropical transients could force equatorially trapped modes. On the other hand, forcing outside the turning latitudes of the extended equatorial modes would not project onto an equatorial mode and would not influence the tropics. Figure 26 provides a schematic depiction of forcing (location Y) that would force an equatorially trapped mode and forcing (at X) that would not. The heavy dashed lines indicate the latitude of the turning latitudes of the k=4, n=1 Rossby mode.

4. CONCLUSIONS

4.1 Observational and Diagnostic Studies

Using the results from diagnostic studies, we can summarize the long-term variability at low latitudes by noting the following points:

- There is considerable coherence between the long term variations from one part of the tropics to other parts of the tropics. At the same time there is a strong correlation between the tropics and higher latitudes but this correlation is a maximum in specific longitudinal belts which coincide with the regions of equatorial upper-tropospheric westerlies, or, the mid-ocean troughs.
- The correlations between the tropics and the extratropics in the vicinity of the mid-ocean troughs are tied strongly to the phase of the ENSO cycle.

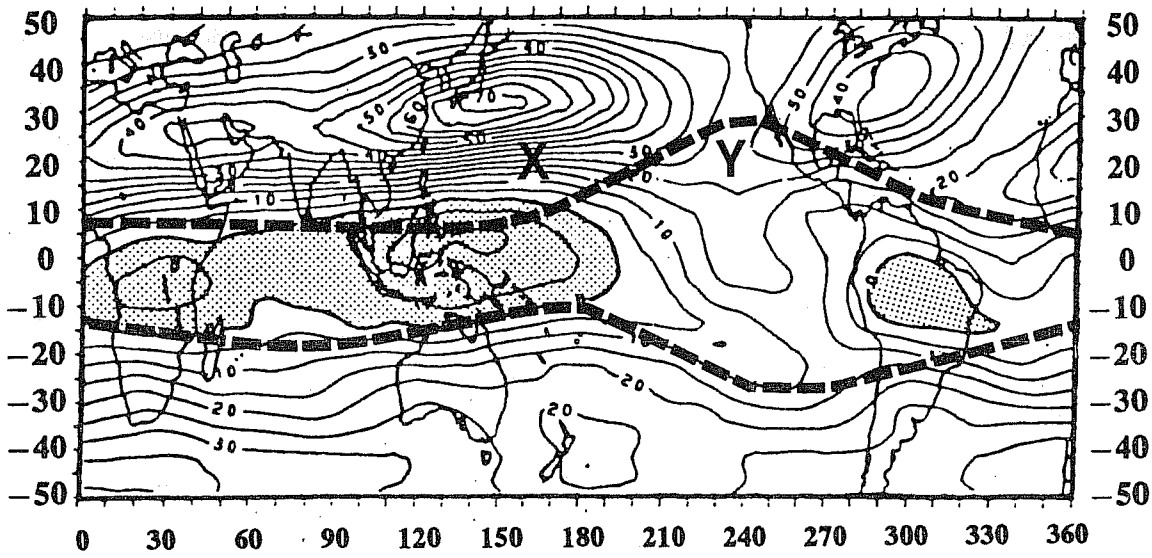

Figure 26: The distribution of the turning latitude of an equatorially trapped wave (dashed line) in the 200 mb boreal winter flow. Letters X and Y denote locations of forcing outside and inside the local turning latitude of the mode, respectively. Forcing located at Y will project onto an equatorial mode. Location X, on the other hand, will not force an equatorial response. From Zhang and Webster (1989).

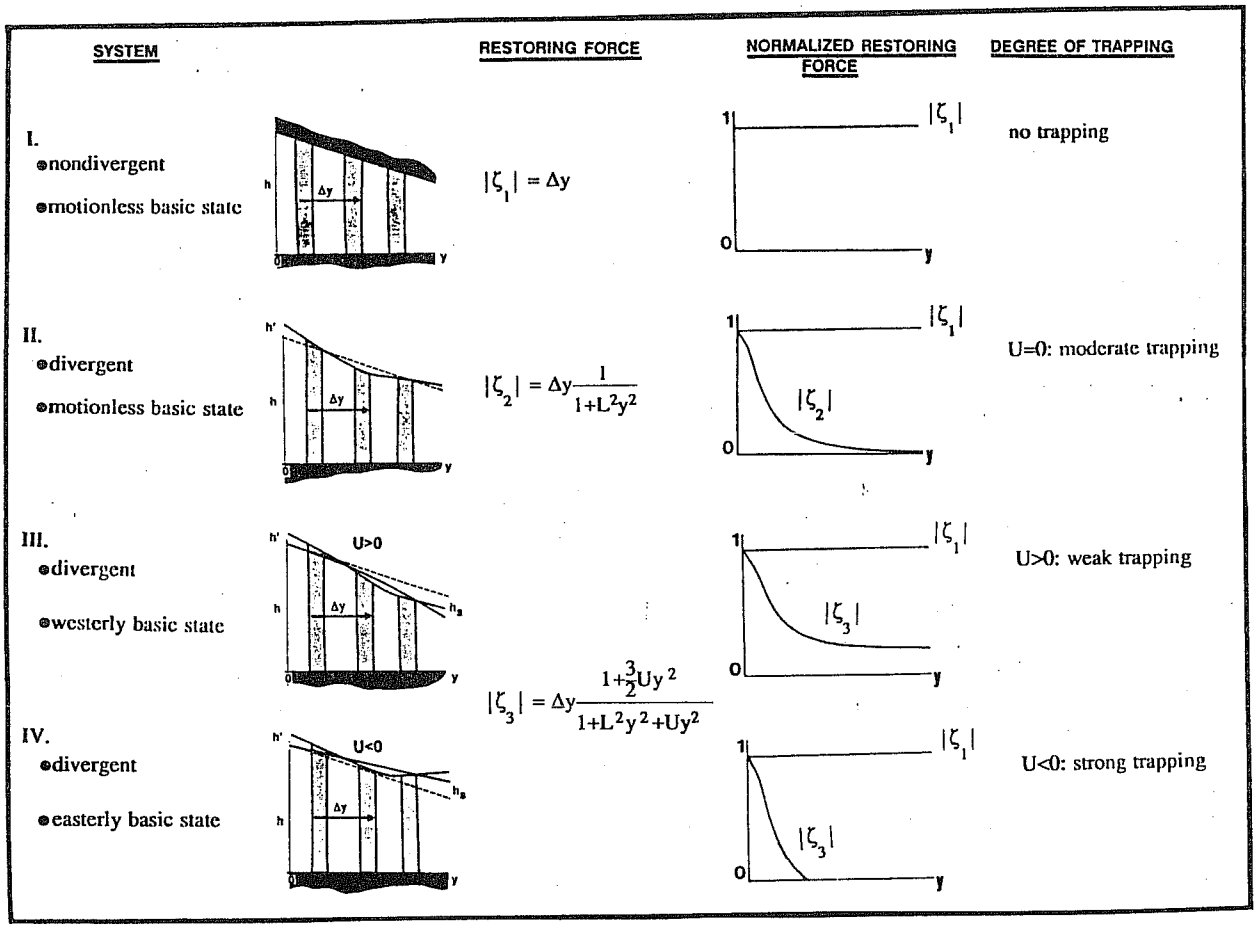

Figure 27: Summary diagram of the physical processes involved in determining the degree of equatorial trapping of a Rossby mode. From Zhang and Webster (1989).

With respect to the relationship of the transient motions relative to the low frequency flow at low latitudes:

- Distinct maxima and minima of *PKE* exist in the tropics which correlate, respectively, with upper tropospheric westerlies and minima with easterlies (Arkin and Webster, 1985, Webster and Yang, 1989). The importance of these correlations is that the tropical mid-ocean trough region is very active in the relative high frequency transients as well as the low frequency evolving background flow.
- The maxima in PKE tend to be in the regions of negative stretching deformation. That is, to the east of the westerly maxima which is consistent with the expectations of Webster and Chang (1988). This association is clearer when the zonal average of the *PKE* is removed and *PKE** examined.

Strong relationships were found between the variations of the summer hemisphere convection and the strength and location of the winter hemisphere jet streams. The main results are summarized as follows:

- The extratropical westerly jet streams in the winter hemisphere are poleward of the tropical OLR minima in the summer hemisphere. During DJF, the jets over Asia, North America and Europe are associated in longitude with the heating maxima over Indonesia, South America, and South Africa, respectively. During JJA, the jet maxima over Australia, South America, and South Africa are associated with the heating maxima over the Asian monsoon regions, North America and North Africa, respectively. These results, presented in Yang and Webster (1990), corroborate the earlier findings of Krishnamurti (1979).
- The location of the major southern hemisphere winter jet stream is keenly associated with the location of the cross-equatorial flow from the convective heating regions of East Asia.
- The annual changes of the intensity of the extratropical westerly jets in the winter hemisphere are in phase with those of the three maximum heating centres in the tropics in the summer hemisphere.
- The variations of the extratropical westerly jet streams, the subtropical meridional wind in the winter hemisphere and the tropical heating in the summer hemisphere are closely associated on an interannual time scale. The tropical heating is important in controlling the year-to-year oscillations of the extratropical westerly jet streams.
- When the heating is strong in the Australian monsoon regions during DJF, the subtropical poleward wind becomes stronger. This leads to a stronger extratropical westerly jet stream over Asia at a location to the west and stronger equatorward wind over the northern central Pacific Ocean. As the stronger heating in those regions increases the longitudinal

heating gradient between the western and central Pacific Ocean, the equatorial westerlies become stronger. During DJF, both the easterlies over the Indonesian regions and the westerlies over the central Pacific Ocean intensify when the heating is stronger over Indonesia. When the maximum heating centre moves eastward and the heating locally weakens in the Australian monsoon regions, the poleward wind becomes weaker and shifts eastward. This may lead to an upstream weakening of the jet when the tropical heating weakens significantly. As the eastward migration of heating increases the latitudinal heating gradient in the central Pacific Ocean, a significant downstream strengthening of the jet may be found. At the same time, the warming of the central Pacific Ocean is accompanied by a weakening equatorward wind in those longitudes over the North Pacific. The Australian monsoon heating and Asian jet stream association is related to the ENSO cycle, especially the changes in the downstream portion of the jet, and is shown in Figure 9b.

- When the heating is stronger in the Asian monsoon regions (especially East Asia) in JJA, the extratropical westerly jet stream over Australia and the subtropical meridional winds over the southern Indian Ocean and the central Pacific Ocean become stronger. When the maximum heating moves eastward and the heating weakens in the Asian monsoon regions, the meridional winds become weaker and shifts eastward. This leads to a remarkable upstream weakening and a significant downstream strengthening of the Australian jet stream together with a weakening equatorward wind over the Southern Central Pacific Ocean. The Asian monsoon heating and Australian jet stream association, stronger than the association between the Australian monsoon heating and the Asian jet in DJF, and more closely related to the ENSO cycle, is shown in Figure 9c.

4.2 Dynamical Studies:

Noting from the observational studies that the slowly evolving basic state contained strong latitudinal shear, longitudinal stretching deformation and vertical shear, we examined the modification of equatorial waves in realistic basic flows. The aim was to see if there was a dynamical basis for the congregation of transient activity in certain regions of the tropics and the regionality of communication between the tropics and the extratropics, and vice versa.

First the impact of variation in the sign and magnitude of a constant basic state was considered. It was found that:

- The non-Doppler effects of a constant basic flow are considerable for the Rossby wave, especially as the scale decreases (see Figs. 12), moderate for the westward mixed Rossby-gravity wave, but insignificant for all other modes. Only the Rossby wave was considered

in this study. A description of the complete equatorial modes is given in Zhang and Webster (1989).

- The impact of the sign of the basic state on the degree of trapping of the mode was considerable. Waves were far less trapped in a westerly flow than in an easterly flow. In westerlies of order 10 ms^{-1} turning latitudes of equatorial modes may extend to 45° latitude compared to about 15 ° in an equivalent easterly (Fig. 13). Thus, one may expect that waves of similar scale would extend much further poleward in the upper troposphere of the eastern Pacific and Atlantic Oceans than elsewhere. A physical rationale for the different degrees of trapping is given Appendix 2.
- The reduction of trapping, or, equivalently, the extension of the turning latitude within the westerly basic state increases considerably with a decrease in longitudinal and latitudinal scale.
- Noting the variation of the mean state of the upper troposphere shown in Fig. 10, it may be expected that waves of similar scale would extend much further poleward in the eastern Pacific and Atlantic Oceans than elsewhere. Such behavior is in keeping with the observations of strong activity and interaction between the tropics and extratropics in these two regions.
- The mid-ocean trough regions are also corridors for the interaction of higher latitude and the tropics. Either modes are able to propagate through the "westerly duct" of Webster and Holton (1982) or extratropical forcing can project onto the extended equatorial mode.

Observations indicate that where there are equatorial westerlies in the upper troposphere that the local lateral shear in the basic state is weak (see *EW* in Fig. 10). On the other hand, where there are easterlies (*EE*), the shear is strong. These observations led to the following conclusions:

- Modes in the shear flow *EE* tend to be considerably more trapped than those in *EW* although the differences are less than those found in the pure easterly and westerly basic states.
- The meridional structures of eastward modes (i.e., the Kelvin, eastwardly propagating gravity modes and the eastward mixed Rossby-gravity mode) appear almost independent of the shear (see Zhang and Webster, 1989). The meridional structures of westward modes are more affected by shear in the manner mentioned above.
- Overall, the impact of shear appears consistent with that found for the constant basic states. Where the shear is strongest and the equatorial flow is easterly, the modes are well trapped about the equator. On the other hand, where the shear is weak and the

equatorial flow is westerly, the trapping is reduced. Thus, one may expect that equatorial transient events will effect the extratropics in the regions of the mid-Pacific and Atlantic trough regions.

We have noted that the longitudinal shearing deformation in the tropics is about the same magnitude as in the middle latitudes. Including horizontal stretching deformation of reasonable magnitude into the model leads to the following conclusions:

- For a wide range of modes, in particular the Rossby family and the westward propagating mixed Rossby-gravity mode, zeros in the Doppler shifted longitudinal group velocity component are possible.
- In a reasonable parameter range, a convergence of transient wave energy occurs in regions where $U_x<0$ occurs. Accumulation into a particular region proceeds from the east ("forward" accumulation) for the long wave packet, and, from the west ("backward" accumulation) for the short wave packet which includes the mixed Rossby-gravity mode. Thus, for a wide range of scales, the westerlies of the upper troposphere of the Pacific and Atlantic Oceans act as "attracters" of transient equatorial modes.
- The phenomena of longitudinal energy accumulation accounts for why there may be regions of transient variance in specific regions of the tropics. Coupled with the impact of the sign and magnitude of the basic state, we can understand why the accumulating modes extend or "emanate" to higher latitudes and why the mid-ocean trough regions are so important in understanding the interaction of the tropics and middle latitudes.

However, the stretching deformation is strongly coupled with vertical shear in the tropical atmosphere. Also, equatorial modes possess a finite vertical group speed. With shear and the vertical group speed taken into account, the following conclusions may be drawn:

- The effects of the vertical propagation of equatorial modes appears to be rather important. Fig. 18a shows that regions of horizontal accumulation correspond to the regions of maximum vertical propagation. This suggestion was supported by the ray tracing through relatively complicated basic flows.
- The mid-ocean trough regions once again emerge as very important regions. Besides being regions where horizontal accumulation occurs for both long and short wave packets, the modes also become less trapped and extend to higher latitudes. The longitudinal variation of vertical shear is so configured as to constrain the modes in the troposphere until they reach the accumulation zone. There, with the change of the sign of the vertical shear, the modes rapidly expand upwards into the stratosphere.

Forcing transients in a model with realistic basic fields in which $U=U(x,y)$ tended to support the conclusions drawn when stretching deformation and lateral shear were considered separately. However, there were a number of specific conclusions:

- There is a strong annual variation in the accumulation and emanation phenomena. The strongest accumulation corresponds, of course, to the times of the year when the equatorial stretching deformation is strongest. Thus, accumulation is a maximum in the eastern Pacific and the central Atlantic Oceans during the boreal winter (DJF) but almost nonexistent during the summer (JJA).
- There is a strong interannual variability of accumulation depending on the magnitude and sign of the SOI. During La Niña times (SOI>>0) the maximum DJF accumulation takes place in the Pacific Ocean. However, during El Niño periods (SOI<<0) when the westerlies are much stronger in the Atlantic than in the Pacific, the region of maximum accumulation changes to the Atlantic.

4.3 Errors and Error Propagation

Observational studies have indicated that there are specific zones of transient activity in the tropical atmosphere and probably well defined corridors of interaction between the tropics and higher latitudes. The theory of equatorial waves, here extended to take into account complicated and realistic basic flows, tends to explain the various observed concentrations of eddy variance.

We noted in the introduction that there was distinct regionality in the climate drift of the NMC model (Fig. 1). Clearly, these error centres correspond to the observed location of the long term average variance in the real atmosphere. Furthermore, they correspond to the regions where theory suggests that there should be an energy accumulation and wave extension or emanation. However, as the climate drift of a model is calculated as a difference field, the regionality of error must result from the accumulation of errors within a particular region.

The model results suggest that there should be a strong temporal variation in the wave propagation and the energy accumulation in the tropics. Perhaps a simple test would be to see if the same temporal variability existed in the climate drift of the model. If it could be shown that error (for example, resulting from the poor parameterization of convection in the warm pool regions of the Pacific Ocean) did propagate in the same manner as the modified transients, then there are two immediate benefits. In the first place, it would suggest a strategy that would help find the source of the errors. Also, if the errors moving away from their source regions obeyed the rules of equatorial waves moving through complicated basic states

it should be possible to anticipate when and where, and if, such errors would be maximized or minimized.

APPENDIX 1: LACK OF GENERALITY OF THE LONG-WAVE APPROXIMATION

Finally, a comment is necessary regarding the "long-wave" approximation (discussed most recently by Stevens *et al.*, 1990) which results from the elimination of the terms with overbars in *(2)* would seem necessary. The dispersion curves for this case are shown as the lighter solid curves for the n = 1, 2 and 3 Rossby modes. The dispersion curves are now linear and deviate rapidly as the horizontal scale decreases. Furthermore, the n=0 mixed Rossby-gravity mode does not exist in the approximate system. The motivation for the approximate set of equations is that they possess an enticing mathematical simplicity and the justification for the approximation comes from the observation that much power resides in the long waves (e.g., k = 0, 1 and 2) in the tropic where $U<<V$. However, this observation only refers to the steady state upper tropospheric tropics which ignores the slowly varying lower tropospheric monsoon circulation where at the equator $V>U$, even in the mean! Also on intraseasonal time scales the majority of power resides in much smaller scales (i.e., $k >$ 5) as pointed out most recently by Liebmann and Hendon (1990). At these scale $U \sim V$. In many parts of the tropics strong "easterly waves" were shown exist. In the warm pool regions, especially in the tropical eastern Indian Ocean and the western Pacific Ocean, virile Rossby and mixed Rossby-gravity modes (i.e., n=0) are regularly found especially during the fall and winter. During the boreal summer strong coherent "surges" occur as part of the Indian monsoon. The scale of the latter two mode types, which are completely ignored in the "long wave approximation" set, is of the order $k \approx 6 - 12$.Clearly, for these scales and for these modes the long-wave approximation is completely inappropriate. Furthermore, we will also see that modes propagating through a basic state which varies in longitude may be required to change their horizontal scale. Thus, a transient wave, which initially has a very large scale, may be modified to a much smaller scale. Thus, when the full complexities of the basic state are taken into account, the "long-wave approximation" may be inappropriate for any scale of motion in the tropics.

APPENDIX 2: EXISTENCE OF EQUATORIALLY TRAPPED MODES

For later reference, the linear nondimensional potential vorticity equation on an equatorial β–plane can be written as:

$$\frac{d\Pi}{dt} = 0 \qquad (A2.1)$$

where Π is the total potential vorticity defined as:

$$\Pi = \zeta(1-\Phi_s) - \phi(\bar{\zeta}+y) + (\zeta \bar{+} y)(1-\Phi_s) \qquad (A2.2)$$

and is the perturbation relative vorticity induced by a latitudinal displacement within an ambient potential vorticity field. Following Pedlosky (1987) we refer to ζ as the *Rossby restoring force* Clearly, ζ will depend strictly upon the ambient PV gradient, and thus on the character of the basic state and on its initial value.

Consider a constant zonal flow, U, so that the potential vorticity, Π, may be written as:

$$\Pi = \zeta(1-\Phi_s) - \phi y + y(1-\Phi_s) \qquad (A2.3)$$

If the initial perturbation potential vorticity of a parcel located at some latitude y_0 is zero, then for a small latitudinal displacement the conservation of potential vorticity states that:

$$y_0(1-\Phi_{s0}) = \zeta(1-\Phi_s) - \phi y + y(1-\Phi_s) \qquad (A2.4)$$

We can then calculate the induced relative vorticity for a number of different basic states.

If the system is non-divergent:

$$\zeta = -\Delta y \qquad (A2.5)$$

so that the restoring force is *independent of latitude* and there is no trapping.

If the basic state is divergent and in motion or at rest, the induced restoring force is given by:

$$\zeta = -\Delta y \left[\frac{1 + \frac{3Uy^2}{2}}{1 + L^2y^2 + Uy^2} \right] \qquad (A2.6)$$

where L is a horizontal scale of a Rossby wave.

Clearly, at a given latitude:

$$|\zeta(U<0)| < |\zeta(U=0)| < |\zeta(U>0)| \qquad (A2.7)$$

Figure 27 provides a schematic view of equatorial trapping in different fluids. For constant zonal flows, the reason for the variation of trapping may be explained in the following manner:

- For $U>0$, the geopotential slope required to maintain the basic flow acts in the same manner as an enhanced β–effect. The orientation of the surface, increases the ambient PV gradient for a poleward displacement. Thus, the induced relative vorticity, the Rossby restoring force, decreases slowly with latitude.

On the other hand;

- For $U<0$, the effective β–effect is reduced. With the necessary slope of the geopotential surface to maintain the easterly, the induced restoring force decreases rapidly with latitude.
- In both the *EE* and *EW* shear flows, the principal impact was to decrease the effect of trapping. Although a solution in term of the PV equation is not easy to obtain, we can understand why trapping is reduced. To maintain the shear in both cases the slope of the surface is enhanced such that the induced relative vorticity for a poleward displacement is enhanced even more. That is, at any given latitude, the restoring force is larger than in a constant zonal flow.

APPENDIX 3: WAVE EQUATION IN STRATIFIED FLOW

Following Lindzen (1967), we rewrite *(11)-(15)* using the following transformations and solutions:

$$\begin{Bmatrix} u \\ v \\ w \\ \rho \\ p \end{Bmatrix} = \begin{Bmatrix} \sqrt{\rho_0}u \\ \sqrt{\rho_0}v \\ \sqrt{\rho_0}w \\ \frac{\rho}{\sqrt{\rho_0}} \\ \frac{p}{\sqrt{\rho_0}} \end{Bmatrix} \sim \begin{Bmatrix} \hat{u}(y,z) \\ \hat{v}(y,z) \\ \hat{w}(y,z) \\ \hat{\rho}(y,z) \\ \hat{p}(y,z) \end{Bmatrix} e^{i(\omega t+kx)} \qquad (A3.1)$$

Put *(A2.1)* into *(11)* and combine them into one equation in term of $\hat{v}$, we can obtain a horizontal structure equation:

$$\left[\frac{d^2}{dy^2}+\frac{k}{\omega}\beta-\frac{k^2\beta^2}{\omega^2}y^2\right]\Psi_n=\left(\frac{1}{gh_n}-\frac{k^2}{\omega^2}\right)(\beta^2y^2-\omega^2)\Psi_n \qquad (A3.2)$$

and a vertical structure equation:

$$\frac{d^2V_n}{d^2z^2}+\frac{\kappa-\epsilon}{H}\frac{d}{dz}\left(\frac{H}{\kappa-\epsilon}\right)\frac{dV_n}{dz}+$$
$$\left[\frac{\kappa-\epsilon}{Hh_n}-\frac{(1-\epsilon)^2}{4H^2}-\frac{(\gamma-\epsilon)}{H}\frac{d}{dz}\left(\frac{\frac{1}{2}(1+\epsilon)-\gamma}{\kappa-\gamma}\right)\right]V_n+\kappa(\kappa-\epsilon)\frac{S_n}{H}=0 \qquad (A3.3)$$

Here we assume that we can separate $\hat{v}$ into two parts:

$$\hat{v}=\sum V_n(z)\Psi_n(y) \qquad (A3.4)$$

where $V_n(z)$ and $\Psi_n(y)$ represent vertical and latitudinal structures of $\hat{v}$ separately. h_n represents a separation constant, $H = \frac{RT_0(z)}{g}$ the scale height of the basic state, $\epsilon(z) = \frac{dH}{dz}$, and $\kappa = \frac{\gamma-1}{\gamma}$. Here we also following Lindzen (1967), assuming that the forcing can be expressed as:

$$\left(\frac{\partial}{\partial y} - \frac{k}{\omega}\beta y\right)\left(\frac{\partial}{\partial z} - \frac{1-\epsilon}{2H}\right)\left(\frac{\sqrt{\rho_0}J}{\kappa-\epsilon}\right) = (\beta^2 y^2 - \omega^2)\sum_n S_n(z)\Psi_n(y) \qquad (A3.5)$$

where S_n represents the vertical structure function of the forcing J.

REFERENCES:

Arkin, P. and P. J. Webster, 1985: Annual and interannual variability of the tropical-extratropical interactions: An empirical study. *Mon. Wea. Rev.*, **113**, 1510–1523.

Blackmon, M. L., J. M. Wallace, N.-C. Lau and S. L. Mullen, 1977:An observational study of the Northern Hemisphere wintertime circulation, *J. Atmos. Sci.*, *34*, 1040–1053, 1977.

Bjerknes, J., 1966: A possible response of the atmospheric Hadley circulation to equatorial anomalies of ocean temperature, *Tellus*, *18*, 820-829.

Bjerknes, J., 1969: Atmospheric teleconnections from the equatorial Pacific, *Mon. Weather Rev.*, *97*, 163-172.

Bolin, B., 1950: On the influence of the earth's orography on the general character of the westerlies, *Tellus*, *2*, 184-196.

Boyd, J. P., 1980: Equatorial solitary waves. Part 1: Rossby solutions. *J. Phys. Oceanogr.*, **10**, 1699–1717.

Boyd, J. P., 1983: Equatorial solitary waves. Part 2: Envelope solutions. *J. Phys. Oceanogr.* **13**, 428–449.

Bretherton, F. P., and C. J. R. Garrett, 1968: Wavetrains in inhomogenous moving media, *Proc. Roy. Soc., London*,**A362**,529–554.

Chang, H.-R., and P. J. Webster, 1990: Energy accumulation and emanation at low latitudes. Part II: Nonlinear response to strong episodic equatorial forcing, *J. Atmos. Sci.*, to appear in November.

Chang, H. –R and P. J. Webster, 1991: Energy accumulation and emanation at low latitudes. Part IV: Influence of realistic basic fields, submitted to *J. Atmos. Sci.*.

Charney, J. G., and A. Eliassen, 1949: A numerical method for predicting the perturbations of the middle latitude westerlies, *Tellus, 1*, 38-54.

Chen, C. -S., and K. E. Trenberth, 1988: Forced planetary waves in the northern hemisphere winter: Wave coupled orographic and thermal forcing, *J. Atmos. Sci.*, *45*, 682–704.

Frederiksen, J. S., and P. J. Webster, 1988: Alternative theories of atmospheric teleconnections and low-frequency fluctuations. *Review of Geophysics*, **26**, 459–494.

Gelaro, R. 1990: PhD Thesis, Department of Meteorology, The Pennsylvania State University.

Held, I. M., 1983: Stationary and quasi-stationary eddies in the extratropical troposphere: Theory, in Large Scale Dynamical Processes in the Atmosphere , edited by B. J. Hoskins and P. R. Pearce, pp. 127-167.

Jacqmin, D., and R. S. Lindzen, 1985: The causation and sensitivity of the northern winter planetary waves, *J. Atmos. Sci.*, *42*, 724-745.

Krishnamurti, T. N., 1979: *Compendium of Meteorology*, vol. 2, part 4–Tropical Meteorology, *Rep.* 364, World Meteorological Organization, Geneva, Switzerland .

Liebmann, B, and H. Hendon, 1990: Synoptic scale disturbances near the equator, *J. Atmos. Sci.*, **47**, 1463–1479.

Lighthill, J., 1978: *Waves in Fluids*, Cambridge University press, 504pp.

Lindzen, R., 1967: Planetary waves on a beta-plane. *Mon. Wea. Rev.* **95**, 441–451.

Manabe, S., and T. B. Terpstra, 1974: The effect of mountains on the general circulation of the atmosphere as identified by numerical experiment, *J. Atmos. Sci.*, **31**, 3-42.

Matsuno, T. 1966: Quasi-geostrophic motions in the equatorial area. *J. Meteor. Soc. Japan*,**44**,25–42.

Maruyama, T., 1967: Large scale disturbances in the equatorial lower stratosphere. *J. Meteor. Soc. Japan*, **45**, 391–407.

Newell, R. E., J. W. Kidson, D. G. Vincent and G. J. Boer, 1974: *The General Circulation of the Tropical Atmosphere and Interactions with Extratropical Latitudes*, MIT Press, 321pp.

O'Lenic, E., P. J. Webster and A. N. Samel, 1985: The effect of initial uncertainty in tropical analysis upon five day forecasts with NMC's global spectral models. NMC Technical Note No. 311.

Pedlosky, J. 1987: *Geophysical Fluid Dynamics*, Springer-Verlig.

Sardeshmukh, P. D. and Hoskins, B. J., 1988: The generation of global rotational flow by steady idealized tropical divergence. *J. Atmos. Sci.*, *45*, 1228–1251.

Simmons, A., J. M. Wallace and G. W. Branstator, 1983: Barotropic wave propagation and instability, and atmospheric teleconnection patterns. *J. Atmos. Sci.*,**40**, 1363–1392.

Stevens, D. E., Kuo, H-. C., W. H. Schubert and P. E. Ciesielski, 1990: Quasi-balanced dynamics in the tropics, *J. Atmos. Sci.*, **47**, 2262–2273.

Wallace, J. M., 1983: The climatological mean stationary waves: Observational evidence, in *Large Scale Dynamical Processes in the Atmosphere*, edited by B. J. Hoskins and P. R. Pearce, pp. 27-52.

Webster, P. J., 1972: Response of the tropical atmosphere to local steady forcing. *Mon. Wea. Rev.*, **100**, 518–540.

Webster, P. J., 1973: Spatial and temporal variability of the steady state response to steady forcing, *Mon. Wea. Rev.*, **101**

Webster, P. J., 1983: The large scale structure of the tropical atmosphere. In Large-Scale Dynamic Processes in the Atmosphere, Eds. B. J. Hoskins and R. pearce, Academic press, 235–276.

Webster, P. J. and H. R. Chang, 1988: Equatorial energy accumulation and emanation regions: Impact of a zonally varying basic state. *J. Atmos. Sci.*, **45**, 803–829.

Webster, P. J. and H. R. Chang, 1991: Equatorial energy accumulation and emanation regions. Part III: Influence of vertical shear, to be submitted to *J. Atmos. Sci.*.

Webster, P. J., and J. R. Holton, 1982: Cross-equatorial response to middle latitude forcing in a zonally varying basic state, *J. Atmos. Sci.*, *39*, 722–733.

Webster, P. J. and S. Yang, 1989: The three-dimensional structure of perturbation kinetic energy and its relationship to the structure of the wind field. *J. Climate*, **2**, 1186–1198..

Whitham, G. B., 1965: A general approach to linear and nonlinear dispersive waves using a Lagrangian, *J. Fluid Mech.*, **22**, 273–283.

Yanai, M. and T. Maruyama, 1966: Stratospheric wave disturbances propagating over the equatorial Pacific. *J. Met. Soc. Japan*, **44**, 291–294.

Yang, S. and P. J. Webster, 1990: The effect of summer tropical heating on the location and intensity of the extratropical westerly jet streams, *J. Geo. Phys. Res.*, **95**, 18705–18721.

Zhang, C. and P. J. Webster, 1989: Effects of zonal flows on equatorially trapped waves. *J. Atmos. Sci.* **46**, 3632–3652.

Zhang , C. and Webster, P. J., 1991: Laterally forced equatorial waves in mean zonal flows. Part I: Stationary Transient Forcing, *J. Atmos. Sci.*, in press.

Zhang , C. and Webster, P. J., 1991: Laterally forced equatorial waves in mean zonal flows. Part II: Propagating Forcing, *J. Atmos. Sci.*, to be submitted.